Quark-meson coupling model, nuclear matter constraints, and neutron star properties

D. L. Whittenbury, J. D. Carroll, and A. W. Thomas
CSSM and ARC Centre of Excellence for Particle Physics at the Terascale, School of Chemistry and Physics, University of Adelaide, Adelaide, South Australia 5005, Australia

K. Tsushima
CSSM and ARC Centre of Excellence for Particle Physics at the Terascale, School of Chemistry and Physics, University of Adelaide, Adelaide, South Australia 5005, Australia
and International Institute of Physics, Federal University of Rio Grande do Norte, Natal, Rio Grande do Norte 59078-400, Brazil

J. R. Stone
Department of Physics, University of Oxford, Oxford OX13PU, United Kingdom
and Department of Physics and Astronomy, University of Tennessee, Knoxville, Tennessee 37996, USA
(Received 19 July 2013; revised manuscript received 17 March 2014; published 3 June 2014)

We explore the equation of state for nuclear matter in the quark-meson coupling model, including full Fock terms. The comparison with phenomenological constraints can be used to restrict the few additional parameters appearing in the Fock terms which are not present at the Hartree level. Because the model is based upon the in-medium modification of the quark structure of the bound hadrons, it can be readily extended to include hyperons and to calculate the equation of state of dense matter in β equilibrium. This leads naturally to a study of the properties of neutron stars, including their maximum mass, radii, and density profiles.

DOI: 10.1103/PhysRevC.89.065801 PACS number(s): 21.65.Cd, 26.60.Kp, 97.60.Jd, 12.39.−x

I. INTRODUCTION

Bulk nuclear matter properties have served as an excellent testing ground for models of baryonic many-body systems for many years. This hypothetical medium possesses many similarities with matter in the interior of heavy nuclei, neutron stars, and core-collapse supernovae. The relative simplicity of the nuclear matter concept, such as the assumption of a uniform density distribution without surface effects, allows the derivation of several key variables which are generally accepted as necessary conditions that must be satisfied by any successful nuclear model.

The uncertainty in the determination of the forces acting among baryons and their modification by the medium has led to a great variety of models. These traditionally start from a bare nucleon-nucleon interaction, fit to experimental data from nucleon-nucleon scattering and the properties of the deuteron, which serves as input to a many-body formalism such as the relativistic Dirac-Bruckner-Hartree-Fock (DBHF) approximation and its nonrelativistic counterpart Bruckner-Hartree-Fock (BHF) [1,2], variational methods [3], correlated basis function models [4], self-consistent Green's function (SCGF) models [5,6], quantum Monte Carlo techniques [7], and chiral effective field theory [8,9]. An alternative is to develop an effective density-dependent baryon-baryon interaction such as the nonrelativistic Skyrme or Gogny interaction, or one of the various relativistic effective Lagrangian models and use it directly in a many-body theory.

With the exception of the role of the Δ excitation in the generation of the three-nucleon force, none of these models consider the internal structure of the nucleon and, in particular, its possible modification in the presence of other hadrons. They depend on a large number of variable parameters which are determined by fitting calculated observables to experimental data. The parameters are often correlated, making it difficult to extract an unambiguous set from such fits, leading to—in principle—an infinite number of such parameter sets [10].

The quark-meson coupling (QMC) model is based upon a very different approach to this problem. Rather than starting with the nucleon-nucleon (NN) force, it begins with the study of a hadron built from quarks immersed in a nuclear medium. The original model, which is employed here, begins with the MIT bag model. One then self-consistently includes the effects of the coupling to the u and d quarks of a scalar-isoscalar meson (σ) mean field, generated by all the other hadrons in the medium, on the internal structure of that hadron. As in earlier boson-exchange models, the σ is a crude but convenient way to simulate the effects of correlated two-pion exchange between hadrons. While the quarks are also coupled to ω and ρ mesons, their Lorentz vector nature means that, at least at the Hartree level, they simply shift quark energies and do not generate nontrivial, density-dependent modifications of the internal structure of the bound hadron.

The QMC model was originally introduced by Guichon [11]. Subsequent development significantly improved the treatment of center-of-mass corrections [12], which had generated an unrealistic amount of repulsion in the original model. This development also included a consistent treatment of finite nuclei, including the spin-orbit force [12]. When applied to Λ hypernuclei, the model provided a very natural explanation of the very small spin-orbit force observed in those systems [13–15]. In an important, recent development, the inclusion of the density dependence of the "hyperfine" interaction between quarks arising from one-gluon exchange (OGE) gave a parameter-free explanation of the empirical absence of medium-mass and heavy Σ hypernuclei, while simultaneously

yielding a good description of Λ hypernuclei [15]. For a review of the many applications of the QMC model, we refer to Ref. [16].

A clear connection has also been established between the self-consistent treatment of in-medium hadron structure and the existence of many-body [17] or density-dependent [18] effective forces. The Skyrme interaction SQMC700, derived in Ref. [18], was among the few percent of Skyrme force that satisfied all the up-to-date constraints on high-density matter up to 3 times nuclear saturation density recently examined by Dutra *et al.* [10]. In particular, in all of the models explored so far involving confined quarks, the self-consistent response to the applied mean scalar field tends to oppose that applied field. This effect can be represented as a "scalar polarizability," which effectively reduces the coupling of the σ to an in-medium baryon as the applied scalar field increases. We stress that this scalar polarizability is a *calculated* property of each hadron and hence introduces no new parameters into the model. Moreover, it is this scalar polarizability which yields the density dependence of the derived Skyrme forces, or equivalently the three-body forces between *all* combinations of hadrons. That is, the model predicts the existence and strength of the three-body forces between not just nucleons, but nucleons and hyperons and hyperons and other hyperons, without additional parameters.

As we have already observed, in a recent development of the QMC model [15], the self-consistent inclusion of the gluonic hyperfine interaction led to a successful description of the binding energies of Λ hypernuclei, as well as the observed absence of medium- and heavy-mass Σ hypernuclei, with no additional parameters. We stress that these results were obtained under the minimal assumption (consistent with the Okubo–Zweig–Iizuka rule) that the σ, ω, and ρ mesons do not couple to strange quarks.

In this paper we present the latest development of the QMC model in which we include the full vertex structure of the exchange term, including not only the Dirac vector term, as was done in Ref. [19], but also the Pauli tensor term. These terms were already included within the QMC model by Krein *et al.* [20] for symmetric nuclear matter and more recently by Ref. [21]. We generalize the work of Krein *et al.* by evaluating the full exchange terms for all octet baryons and adding them, as additional contributions, to the energy density. A consequence of this increased level of sophistication is that, if we insist on using the hyperon couplings predicted in the simple QMC model, with no coupling to the strange quarks, the Λ hyperon is no longer bound.

The present paper compliments the work of Ref. [21] which also considered the tensor interaction in a variation of the QMC model by investigating an extended set of nuclear matter properties with comparisons to heavy-ion collision data and other theoretical models. The present version of the QMC model differs from that of Ref. [21] as we use couplings as derived within the model and treat contact terms differently. As is very well known from quantum hadrodynamics [22,23] and QMC [20] Hartree-Fock calculations the scalar $\Sigma^s(k)$ and temporal vector $\Sigma^0(k)$ self-energy components are essentially independent of momentum and the spatial vector component is very small. For these reasons we make the assumption that the self-consistency can be treated approximately as in Ref. [19] and as in Ref. [20], where the latter included a Fock correction to the scalar field. To state this more precisely, we neglect the small spatial vector component of the self-energy such that $\vec{k}^* = \vec{k} + \hat{k}\Sigma^v(k) \simeq \vec{k}$ and the remaining components are treated as momentum independent. This approximate self-energy,

$$\begin{aligned}\Sigma(k) &= \Sigma^s(k) - \gamma^0\Sigma^0(k) + \vec{\gamma}\cdot\vec{k}\Sigma^v(k)\\ &\simeq \Sigma^s - \gamma^0\Sigma^0, \end{aligned} \tag{1}$$

has a form identical to the usual mean-field (Hartree) result and the Fock corrections to these components can be included by requiring thermodynamical consistency, which amounts to minimizing the total energy density with respect to the meson fields. This results in a small correction to the scalar field.

In Sec. II we present the basic features of the QMC model used in this work. The application of the model leading to the equation of state (EoS) of dense matter and a description of its parameters is given in Sec. III A. Results obtained for infinite nuclear matter, symmetric and asymmetric, as well as β-equilibrium matter are followed by those for cold neutron stars and their comparison with experimental and observational constraints can be found in Secs. III B–III E. The main results, sensitivity of the EoS and related quantities to variation of some model parameters, are summarized in Sec. III F. We then make a comparison between the present work and recent variations of the QMC model studied in Refs. [21,24] and others in Sec. III G. Discussion and concluding remarks are presented in Sec. IV.

II. THE QMC MODEL

The QMC model is based upon the self-consistent modification of the structure of a baryon embedded in nuclear matter. It is a relativistic mean-field model which incorporates the internal quark structure of the baryons, represented as MIT bags containing three quarks in a color-singlet configuration. Interactions occur between quarks in distinct bags via the exchange of mesons coupled locally to the quarks.

Thus, in addition to the usual terms in the Lagrangian density of the MIT bag, the QMC model adds the simplest local couplings of σ, ω, and ρ mesons to the confined quarks. That is, the couplings are $g^q_\sigma \bar{q} q \sigma$, $g^q_\omega \bar{q}\gamma^\mu q \omega_\mu$, and $g^q_\rho \bar{q}\gamma^\mu \frac{\vec{\tau}}{2} q \cdot \vec{\rho}_\mu$, respectively [11,12]. Here q represents the SU(2) doublet of u and d quarks and the coupling of these mesons to the s quark is taken to be zero. These QMCs describe the interaction between quarks in *different* hadrons. They act as the source of mean fields in medium as well as serving to modify the equation of motion of the confined quarks. This leads to a self-consistency problem which is highly nontrivial for the scalar field, whereas the vector couplings in uniform, infinite nuclear matter involve only time components—e.g., $\omega^\mu = \bar{\omega}\delta^{\mu 0}$—and so they simply shift energy levels. As a result, the effective strength of the coupling of the scalar meson to a hadron containing light quarks is suppressed as the scalar field increases, or equivalently, as the density increases. Thus, as a result of this self-consistent calculation at the quark level, one can express the in-medium baryon masses, M^*_B,

as functions of the scalar field (as in Ref. [15]) through a calculated, density-dependent, scalar coupling, $g_{\sigma B}(\bar{\sigma})$.

The saturation of symmetric nuclear matter [11] is a natural effect of the self-consistent response of the quark wave functions to the mean scalar field, a direct consequence of which is the reduction of the effective σN coupling as the σ field increases. By analogy with the electric polarizability of an atom, which tends to arrange its internal structure to oppose an applied electric field, this reduction of the σN coupling is characterized as the scalar polarizability of the nucleon. It is remarkable that the influence of baryon substructure, in a mean-field approximation, is entirely described in terms of the parametrization of the effective mass of the baryon through the density-dependent scalar coupling derived from the quark model of the baryon and g_σ^q. One can therefore replace the explicit description of the internal structure of the baryons by constructing an effective Lagrangian on the hadronic level, with the calculated nonlinear σ-baryon couplings given in Ref. [15],

$$M_B^* = M_B - w_{\sigma B} g_{\sigma N} \bar{\sigma} + \frac{d}{2} \tilde{w}_{\sigma B} (g_{\sigma N} \bar{\sigma})^2 \tag{2}$$

(where the weightings $w_{\sigma B}$ and $\tilde{w}_{\sigma B}$ simply allow the use of a unique coupling to nucleons), and proceed to solve the relativistic mean-field equations in a standard way [22].

The QMC Lagrangian density used in this work is given by a combination of baryon, meson, and lepton components,

$$\mathcal{L} = \sum_B \mathcal{L}_B + \sum_m \mathcal{L}_m + \sum_\ell \mathcal{L}_\ell, \tag{3}$$

for the octet of baryons $B \in \{N, \Lambda, \Sigma, \Xi\}$, selected mesons $m \in \{\sigma, \omega, \rho, \pi\}$, and leptons $\ell \in \{e^-, \mu^-\}$ with the individual Lagrangian densities,

$$\mathcal{L}_B = \bar{\Psi}_B \big[i\gamma_\mu \partial^\mu - M_B + g_{\sigma B}(\sigma)\sigma - \Gamma^\mu_{\omega B}\omega_\mu - \vec{\Gamma}^\mu_{\rho B} \cdot \vec{\rho}_\mu - \vec{\Gamma}_{\pi B} \cdot \vec{\pi} \big] \Psi_B, \tag{4}$$

$$\sum_m \mathcal{L}_m = \frac{1}{2}\big(\partial_\mu \sigma \partial^\mu \sigma - m_\sigma^2 \sigma^2\big) - \frac{1}{4}\Omega_{\mu\nu}\Omega^{\mu\nu} + \frac{1}{2} m_\omega^2 \omega_\mu \omega^\mu - \frac{1}{4}\vec{R}_{\mu\nu} \cdot \vec{R}^{\mu\nu} + \frac{1}{2} m_\rho^2 \vec{\rho}_\mu \cdot \vec{\rho}^\mu + \frac{1}{2}\big(\partial_\mu \vec{\pi} \cdot \partial^\mu \vec{\pi} - m_\pi^2 \vec{\pi} \cdot \vec{\pi}\big), \tag{5}$$

for which the vector meson field strength tensors are $\Omega_{\mu\nu} = \partial_\mu \omega_\nu - \partial_\nu \omega_\mu$ and $\vec{R}_{\mu\nu} = \partial_\mu \vec{\rho}_\nu - \partial_\nu \vec{\rho}_\mu$, and

$$\mathcal{L}_\ell = \bar{\Psi}_\ell (i\gamma_\mu \partial^\mu - m_\ell) \Psi_\ell. \tag{6}$$

For the baryon masses we take the average over the isospin multiplet of their experimental values, where as for the mesons and leptons we simply use the experimental values.

In a mean-field description of infinite nuclear matter with uniform density, one can set spatial derivatives of all fields to zero and replace the meson field operators with their expectation values:

$$\sigma \to \langle \sigma \rangle \equiv \bar{\sigma}, \tag{7}$$

$$\omega_\mu \to \langle \omega_\mu \rangle = \langle \delta_{\mu 0} \omega_\mu \rangle \equiv \bar{\omega}, \tag{8}$$

$$\vec{\rho}_\mu \to \langle \vec{\rho}_\mu \rangle = \langle \delta_{\mu 0} \delta_{a3} \rho_{\mu a} \rangle \equiv \bar{\rho}, \tag{9}$$

$$\vec{\pi} \to \langle \vec{\pi} \rangle = 0. \tag{10}$$

This is usually called the Hartree mean-field approximation.

The next step is to include the Fock level contributions involving the meson-baryon vertices which are expressed as

$$\Gamma_{\sigma B} = g_{\sigma B} C_B(\bar{\sigma}) F^\sigma(k^2)\mathbf{1} = -\frac{\partial M_B^*}{\partial \bar{\sigma}} F^\sigma(k^2)\mathbf{1}, \tag{11}$$

$$\vec{\Gamma}_{\eta B} = \epsilon_\eta^\mu \vec{\Gamma}_{\mu\eta B} = \epsilon_\eta^\mu \left[g_{\eta B}\gamma_\mu F_1^\eta(k^2) + \frac{i f_{\eta B} \sigma_{\mu\nu}}{2M_B^*} k^\nu F_2^\eta(k^2) \right] \vec{t}; \quad \eta \in \{\omega, \rho\}, \tag{12}$$

$$\vec{\Gamma}_{\pi BB'} = i g_{\pi BB'} F^\pi(k^2) \gamma^\mu k_\mu \gamma_5 \vec{\tau}, \tag{13}$$

with the isospin matrix $\vec{t}$ only applicable to isovector mesons. For nucleons and cascade particles $\vec{t} = \frac{\vec{\tau}}{2}$. For the ρ meson the flavor dependence is contained completely in the isospin matrix, such that $g_{\rho B} = g_{\rho N} = g_\rho$. The pion-baryon interaction is assumed to be described by an SU(3) invariant Lagrangian with the mixing parameter $\alpha = 2/5$ [19] from which the hyperon-pion coupling constants can be given in terms of the pion-nucleon coupling, $g_{\pi BB'} = g_{\pi NN}\chi_{BB'} = \frac{g_A}{2f_\pi}\chi_{BB'}$ [19,25].

The ratios of tensor to vector couplings $\kappa^B_{(\omega,\rho)} = f_{B(\omega,\rho)}/g_{B(\omega,\rho)}$ given in Table I are rescaled using the free proton mass

$$\kappa^B_{(\omega,\rho)} \to \kappa^B_{(\omega,\rho)} \times \frac{M_B^*}{M_p}. \tag{14}$$

Equation (14) is used in all variants of the model ("scenarios"), considered in this work except where a result is labeled "Eff. Proton Mass." The reason for this choice is that the derivation of the QMC model is based on an order-by-order expansion in the effect of the scalar field; using the effective mass of the proton in the Pauli term coupling assumes that the scalar field does not appear in some other way at the level of momentum-dependent couplings. A systematic expansion would ensure that all effects are included consistently to a given order. In the absence of such a derivation it would be natural to write the couplings in terms of the free baryon mass as is done in

TABLE I. Relations between baryon magnetic moments and anomalous isoscalar and isovector magnetic moments $\kappa^B_{(IS,IV)} =: \kappa^B_{(\omega,\rho)} = f_{B(\omega,\rho)}/g_{B(\omega,\rho)}$ using experimental magnetic moments [29].

Relation	Magnetic moments (nm)	$\kappa^B_{(IS,IV)} =: \kappa^B_{(\omega,\rho)}$
$\mu_p = 1 + \frac{1}{2}(\kappa^N_{IS} + \kappa^N_{IV})$	$\mu_n = -1.913$	$\kappa^N_{IS} = -0.12$
$\mu_n = \frac{1}{2}(\kappa^N_{IS} - \kappa^N_{IV})$	$\mu_p = 2.793$	$\kappa^N_{IV} = 3.706$
$\mu_\Lambda = \kappa^\Lambda_{IS}$	$\mu_\Lambda = -0.61$	$\kappa^\Lambda_{IS} = -0.61$
$\mu_{\Sigma^+} = 1 + (\kappa^\Sigma_{IS} + \kappa^\Sigma_{IV})$	$\mu_{\Sigma^-} = -1.16$	$\kappa^\Sigma_{IS} = 0.649$
$\mu_{\Sigma^-} = -1 + (\kappa^\Sigma_{IS} - \kappa^\Sigma_{IV})$	$\mu_{\Sigma^+} = 2.458$	$\kappa^\Sigma_{IV} = 0.809$
$\mu_{\Xi^0} = \frac{1}{2}(\kappa^\Xi_{IS} + \kappa^\Xi_{IV})$	$\mu_{\Xi^-} = -0.65$	$\kappa^\Xi_{IS} = -0.9$
$\mu_{\Xi^-} = -1 + \frac{1}{2}(\kappa^\Xi_{IS} - \kappa^\Xi_{IV})$	$\mu_{\Xi^0} = -1.25$	$\kappa^\Xi_{IV} = -1.5993$

Ref. [21,26] and not include just one effect of the scalar field at this order.

The σ, ω, ρ, and π form factors are all taken to have the dipole form $F(k^2) \simeq F(\vec{k}^2)$ with the same cutoff Λ. Clearly, these form factors are only of concern for the Fock terms. We make specific note of the two terms which contribute to the vector meson vertices, a vector "Dirac" term and a tensor "Pauli" term.

Through the Euler-Lagrange equations, we obtain from this Lagrangian density a standard system of coupled, nonlinear partial differential equations for the meson mean fields [12]. Meson retardation effects are not included and contact terms are subtracted; see the Appendix for details. We note that the mean-field approximation becomes progressively more reliable with increasing density. Finally, we note that we have also neglected any modification of the Dirac sea of negative energy states with increasing density (see, however, the discussion of such effects within the NJL model in Ref. [27]).

III. EQUATION OF STATE OF BARYONIC MATTER

A. Formalism

The EoS relates energy density, pressure, and temperature to baryon number densities ρ_B. In this work, we include contributions from the full baryon octet in the limit $T = 0$. The total energy density is given as a sum of the baryonic, mesonic, and leptonic contributions,

$$\epsilon_{\text{total}} = \epsilon_B + \epsilon_{\sigma\omega\rho} + \epsilon_F + \epsilon_\ell. \tag{15}$$

The nonleptonic energy density can be divided into a direct (Hartree) part, $\epsilon_H = \epsilon_B + \epsilon_{\sigma\omega\rho}$, where

$$\epsilon_B = \frac{2}{(2\pi)^3} \sum_B \int_{|\mathbf{p}|\leqslant p_F} d\mathbf{p} \sqrt{p^2 + M_B^{*2}}, \tag{16}$$

$$\epsilon_{\sigma\omega\rho} = \sum_{\alpha=\sigma,\omega,\rho} \frac{1}{2} m_\alpha^2 \bar{\alpha}^2, \tag{17}$$

where $\bar{\alpha}$ refers to the mean-field value of meson α, plus an exchange (Fock) contribution

$$\epsilon_F = \frac{1}{(2\pi)^6} \sum_{m=\sigma,\omega,\rho,\pi} \sum_{BB'} C^m_{BB'} \int_{|\mathbf{p}|\leqslant p_F} \int_{|\mathbf{p}'|\leqslant p_{F'}} d\mathbf{p} d\mathbf{p}' \Xi^m_{BB'}. \tag{18}$$

The coefficients $C^\sigma_{BB'} = C^\omega_{BB'} = \delta_{BB'}$, $C^\rho_{BB'}$, and $C^\pi_{BB'}$, which arise from symmetry considerations, are given in Ref. [19]. This nonleptonic energy density is then given by $\epsilon_{\text{hadronic}} = \epsilon_H + \epsilon_F = \epsilon_B + \epsilon_{\sigma\omega\rho} + \epsilon_F$. Note that the pion contributes only at exchange level as parity considerations lead to a vanishing direct level contribution. It nonetheless plays an important role in reducing the incompressibility of nuclear matter [19].

The leptonic energy density is simply

$$\epsilon_\ell = \frac{2}{(2\pi)^3} \sum_\ell \int_{|\mathbf{p}|\leqslant p_{F,\ell}} d\mathbf{p} \sqrt{p^2 + m_\ell^2}. \tag{19}$$

The scalar mean field in Eq. (17) is calculated self-consistently as

$$\bar{\sigma} = -\frac{1}{m_\sigma^2} \frac{\partial \epsilon_H}{\partial \bar{\sigma}} - \frac{1}{m_\sigma^2} \frac{\partial \epsilon_F}{\partial \bar{\sigma}} \tag{20}$$

$$= -\frac{2}{m_\sigma^2 (2\pi)^3} \sum_B \int_{|\mathbf{p}|\leqslant p_F} d\mathbf{p} \frac{M_B^*}{\sqrt{p^2 + M_B^{*2}}} \frac{\partial M_B^*}{\partial \bar{\sigma}} - \frac{1}{m_\sigma^2} \frac{\partial \epsilon_F}{\partial \bar{\sigma}}, \tag{21}$$

where the second term in Eq. (21) is the Fock level correction to the scalar field, which is included in the scenarios "Fock $\delta\sigma$" and "Eff. Proton Mass + $\delta\sigma$." The vector meson mean fields simply scale with either the total or isovector baryonic density

$$\bar{\omega} = \sum_B \frac{g_{\omega B}}{m_\omega^2} \rho_B, \tag{22}$$

$$\bar{\rho} = \sum_B \frac{g_{\rho B}}{m_\rho^2} I_{3B} \rho_B, \tag{23}$$

where I_{3B} is the third component of isospin for baryon B.

For ϵ_F, shown in Eq. (18), the integrand has the form

$$\Xi^m_{BB'} = \frac{1}{2} \sum_{s,s'} |\bar{u}_{B'}(p',s') \Gamma_{mBB'} u_B(p,s)|^2 \Delta_m(\mathbf{k}), \tag{24}$$

where $\Delta_m(\mathbf{k})$ is the Yukawa propagator for meson m with momentum $\mathbf{k} = \mathbf{p} - \mathbf{p}'$, and u_B are the baryon spinors. The integrands are presented in the Appendix.

The expression for total energy density is therefore dependent on just the three main adjustable coupling constants, which control the coupling of the mesons to the two lightest quarks, g^q_σ, g^q_ω, and g^q_ρ for $q = u,d$ ($g^s_\alpha = 0$ for all mesons α). In addition, one has the meson masses, the value of the cutoff parameter Λ appearing in the dipole form factors needed to evaluate the Fock terms and finally the bag radius of the free nucleon. The σ, ω, and ρ couplings to the quarks are constrained to reproduce the standard empirical properties of symmetric ($N = Z$) nuclear matter: the saturation density $\rho_0 = 0.16$ fm^{-3}, the binding energy per nucleon at saturation of $\mathcal{E}(\rho = \rho_0) = -15.865$ MeV, as well as the asymmetry energy coefficient $a_{\text{asym}} \equiv S_0 \equiv S(\rho_0) = 32.5$ MeV [19] (see also Sec. III C).

The ω, ρ, and π meson masses are set to their experimental values. The ambiguity in defining the mass of the σ after quantizing the classical equations of motion was explained in detail in Ref. [12]. Here it is set to the value that gave the best agreement with experiment for the binding energies of finite nuclei in a previous QMC model calculation [18], which was 700 MeV. This is a common value taken for the σ meson mass which is generally considered in RMF models to be in the range 400–800 MeV.

The form factor cutoff mass, Λ, controls the strength of the Fock terms Eqs. (11)–(13). We considered a range of values, $0.9 \text{ GeV} \leqslant \Lambda \leqslant 2.0$ GeV, with the preferred value, as we shall see, being 0.9 GeV. For simplicity we have used the same cutoff for all mesons. Because the pion mass is much lower than that of the other mesons, we have confirmed that using a lower cutoff for the pion does not significantly influence the

results. This is not surprising as Fock terms are expected to be more significant at higher density, where we have found that the pion does not contribute greatly.

All the other coupling constants in the expression for the total energy density are *calculated* within the QMC model or determined from symmetry considerations without further need for adjustable parameters. The one exception is $g_{\sigma B}(\bar{\sigma})$, which shows a weak dependence on the free nucleon radius $R_N^{\rm free}$. We checked that changes of order 20% in $R_N^{\rm free}$, consistent with nucleon properties, have no significant effect on the properties of nuclear matter and chose $R_N^{\rm free} = 1.0$ fm.

The baryon-meson coupling constants $g_{\sigma N}(0)$, $g_{\omega B}$, and $g_{\rho B}$ (or equivalently the three QMC constants) are determined by fitting the saturation properties of symmetric nuclear matter. Only $g_{\sigma B}$ is density dependent and that dependence is calculated self-consistently according to

$$\frac{\partial}{\partial\bar{\sigma}}\left[g_{\sigma B}(\bar{\sigma})\bar{\sigma}\right] = g_{\sigma B}(0)\,C_B(\bar{\sigma}) = -\frac{\partial M_B^*}{\partial\bar{\sigma}} \equiv -\frac{\partial M_B^*\left(\bar{\sigma}, g_{\sigma N}, R_N^{\rm free}\right)}{\partial\bar{\sigma}}, \tag{25}$$

where M_B^* is calculated in the QMC model using the MIT bag with OGE for the baryon structure. The couplings $g_{\omega B}$ and $g_{\rho B}$ are expressed in terms of the quark level couplings as

$$g_{\omega B} = n_{u,d}^B g_\omega^q, \quad g_{\rho B} = g_{\rho N} = g_\rho^q, \tag{26}$$

where $n_{u,d}^B$ is the number of light quarks in baryon B.

At densities $\sim$2–3ρ_0 one expects, simply because the Fermi level of the neutrons rises rapidly, that for matter in β-equilibrium hyperons must be considered. There are very few experimental data on the N-Y and Y-Y interactions, which makes the traditional approach through phenomenological pairwise interactions very difficult. There is certainly no hope of determining the relevant three-body forces which are expected to be critical at high density. One of the attractive features of the QMC model is that it predicts all of these forces in terms of the underlying QMCs, the scalar meson mass, and the particular quark model chosen (the MIT bag here). Furthermore, the density dependence of the scalar couplings to each baryon is also determined by the bag model mass parametrization. The inclusion of this density-dependent, in-medium interaction is equivalent in a density-independent framework to including the appropriate three-body force between all baryons.

Remarkably, in the absence of the Pauli Fock terms, the model predicted realistic Λ binding energies and, at the same time, realistic Σ repulsion in matter [15]. As we show later in Sec. III F, the additional repulsion associated with the Fock term is not adequately compensated and the agreement is lost. In this work we assess the magnitude of the needed change by artificially modifying the σ couplings for the hyperons to match the empirical observations. This procedure will serve as a guidance in the future development of the model, as outlined in Sec. IV

It is well known that the coupling of the ρ meson to a particular baryon has a relatively large Pauli, or tensor, coupling [i.e., $f_{\rho B}$ in Eq. (12)]. The value used varies from one model of the nuclear force to another. In the QMC model the prediction of the tensor coupling at zero momentum transfer is unambiguous; it is exactly the anomalous, isovector magnetic moment of the baryon in the MIT bag model. Similarly, the tensor coupling of the ω, which in the case of the nucleon is much smaller than for the ρ, is determined by the isoscalar magnetic moment. Because the MIT bag model reproduces the experimental values of the magnetic moments quite well, the tensor coupling required within the QMC model is equivalent to using vector meson dominance [28] and in practice we use values for the magnetic moments from the Particle Data Group [29]. Finally and purely as an exercise aimed at exploring the model dependence, we consider two different choices for the ratios of tensor to vector coupling constants $f_{\alpha B}/g_{\alpha B}$, with $\alpha \in \{\rho,\omega\}$. Whereas, as we explained, in the standard QMC calculation we take $f_{\rho N}/g_{\rho N} = 3.70$, we also explore the consequences of arbitrarily setting $f_{\rho N}/g_{\rho N} = 5.68$ in the "Increased $f_{\rho N}/g_{\rho N}$" scenario. In this scenario we arbitrarily take the ratios of tensor to vector couplings of all baryons from the Nijmegen potentials (Table VII of Ref. [30]).

The only other parameters in the QMC model are those entering the bag model. We refer the reader to Ref. [15], where those parameters were obtained. None of them have been adjusted to any property of nuclear matter, although all calculations involving the QMC model at present rely on the MIT bag model with OGE and could be, in principle, improved upon by using a more sophisticated model of quark confinement. Nonetheless, with this simple quark-based model, remarkable agreement with a broad range of experimental data has been obtained [16].

Having established the QMC model parameters, in the following section we calculate properties of symmetric (SNM) and pure neutron (PNM) nuclear matter as well as matter in β equilibrium (BEM). The latter consists of nucleons and leptons, while matter in generalized β equilibrium (GBEM) contains the full baryon octet and leptons. Using the derived EoS, we calculate the properties of cold neutron stars and make a comparison with up-to-date experimental and observational data. We also examine the robustness of those results on the limited number of parameters entering the model.

B. Infinite symmetric and pure neutron nuclear matter

A minimal set of saturation properties of symmetric nuclear matter, the saturation density, the binding energy per particle, and the symmetry energy at saturation, were used to fix the QMC constants as described in Sec. III A. None of those properties is actually an *empirical* quantity, because they are not measured directly but extracted from experiments or observations in a model-dependent way. However, there is a general consensus that all meaningful theories of nuclear matter should reproduce these quantities correctly. Moreover, other properties of both symmetric and pure neutron matter, derived from derivatives of the energy per particle with respect to particle number density, together with their density dependence, can be compared to empirical data to further test the theories. These include the pressure, incompressibility (compression modulus), and slope of the symmetry energy.

Let us define the hadronic energy per particle, $E = \epsilon_{\rm hadronic}/\rho$, where ρ is the total baryonic density and define

the following quantities as a function of ρ. The first derivative of E provides an expression for baryonic pressure,

$$P = \rho^2 \frac{\partial E}{\partial \rho}. \tag{27}$$

The second derivative of E is the compression modulus or incompressibility,

$$K = 9\rho^2 \left(\frac{\partial^2 E}{\partial \rho^2} \right). \tag{28}$$

The third derivative defines the so-called skewness coefficient (some authors define $K' = -Q$):

$$Q = 27\rho^3 \left(\frac{\partial^3 E}{\partial \rho^3} \right). \tag{29}$$

These quantities can be evaluated at any density and any proton/neutron asymmetry ratio $\beta = (\rho_n - \rho_p)/\rho$ at which the model for the baryonic energy per particle is valid. The particular values at saturation density, ρ_0, are indicated with a subscript zero (e.g., K_0, Q_0, etc.). In SNM, $\rho_n = \rho_p = 1/2\rho$, the values of the incompressibility and skewness at saturation density can be compared to experiment. Obviously, the pressure at saturation density is equal to zero. It is convenient to express the density dependence of the energy per particle in SNM as a Taylor expansion of E about the saturation density in terms of a variable $x = (\rho - \rho_0)/3\rho_0$,

$$E_{\mathrm{SNM}}(\rho) = E_0 + \tfrac{1}{2} K_0 x^2 + \tfrac{1}{6} Q_0 x^3 + \mathcal{O}(x^4). \tag{30}$$

The value of the incompressibility of infinite nuclear matter at saturation density has been the subject of considerable debate for several decades. It can be extracted either from measurement of energies of giant monopole resonances (GMRs) in spherical nuclei or calculated theoretically in nonrelativistic and relativistic models, typically involving mean- field plus random-phase approximation (see, e.g., Refs. [31–33]). The consensus has gravitated to a value of $K_0 = 240 \pm 20$ MeV, as calculated in nonrelativistic approaches, although somewhat higher values are predicted in relativistic models. Recent reanalysis of experimental data on GMR energies in nuclei with $56 < A < 208$, in an empirical approach [33] showed that K_0 critically depends on properties of the nuclear surface and the most likely values of K_0 are between 250 and 315 MeV.

There is no rigorous constraint available for the skewness coefficient except for the results of Farine *et al.* [34]. They obtained a model-dependent value $K' = 700 \pm 500$ MeV from an analysis of the nuclear breathing mode, using a selection of Skyrme forces.

We now give details of how the optical potentials of hyperons embedded in SNM are calculated. We refrain from discussing these results until Sec. III D as these potentials are intimately connected to the particle content of matter in generalized β equilibrium and are therefore more naturally discussed there. In many works optical potentials for the hyperons in SNM are evaluated and used to constrain hyperon coupling constants. In the QMC model these couplings are derived within the model. We make the following approximation to evaluate the optical potentials in SNM at saturation density. For each hyperon a small number density is chosen, so that we can evaluate their chemical potential numerically via Eq. (45). A small density means that this chemical potential is approximately the energy of a zero momentum hyperon embedded in symmetric nucleon only matter. We can then calculate the optical potentials by $U_i(\rho_0) = \mu_i - M_i$. These values are tabulated in Table II for the Λ, Σ^-, and Ξ^- hyperons.

In PNM, $\rho_n = \rho$ and $\rho_p = 0$. Although PNM does not exist in nature, it is seen as a first approximation to matter in the outer core of neutron stars at densities higher than ρ_0. The density dependence of the energy per particle of PNM is poorly known, except for the fact that PNM does not bind; i.e., the energy per particle is positive at all densities.

At very low densities, below $\sim 0.1\ \rho_0$, experiments with cold Fermi atoms have yielded information about strongly interacting fluids, similar to low-density matter in neutron star crusts. Dutra *et al.* [10] studied these constraints in detail. In this work we concentrate on the higher-density region, above $\sim 0.1\ \rho_0$, as the QMC model may have limited applicability at very low densities. In the absence of experimental data in this density region we can only use theory for a comparison.

Very recently, Tews *et al.* [35] presented the first complete next-to-next-to-next-to-leading-order ($\mathrm{N^3LO}$) calculation of the PNM energy, and Hebeler and Furnstahl [36] investigated the energy per particle in PNM at subsaturation densities using two- and three-nucleon chiral effective field theory (CEFT) interactions that were consistently evolved within the framework of the similarity renormalization group. We compare their results with the QMC predictions in Fig. 1. Clearly, the QMC prediction for the density dependence of the energy per particle in PNM is very similar to that of Tews *et al.* [35] at subsaturation density, with a somewhat steeper increase at densities above saturation.

An interesting connection has been made between the pressure in the PNM neutron skin in heavy nuclei and the radius and crust thickness of a cold neutron star [37]. Thus, a microscopic theoretical calculation of the PNM pressure became of interest, in particular at subsaturation densities. Tsang *et al.* (see Fig. 4 and related references in Ref. [38]) collected several recent calculations of the PNM pressure as a function of particle number density. We show in Fig. 2 a selection of the models: BHF with Av18 two-body potential [39], quantum Monte Carlo (QuMoCa) with Av8′ two-body potential [40], and CEFT [9]. The main uncertainty in these calculations is the strength of three-body forces, which clearly make a significant contribution to the total pressure in these models (compare the left and right panels of Fig. 2, with the QMC result shown in the right panel). The QMC model, which naturally includes three-body forces without additional parameters (see Sec. IV), indicates a somewhat faster growth of pressure with increasing density than the other three-body interactions.

Limits for the pressure-density relationship in SNM and PNM in the density region $2–5\rho_0$ have been inferred from a comparison of experimental data on matter flow in energetic heavy ion collisions and predictions of a dynamical transport theory by Danielewicz *et al.* (see Ref. [41] and references therein). The matter created in the collision, lasting $\sim 10^{-23}$ s at an incident kinetic energy per nucleon varying from about 0.15

TABLE II. Couplings, nuclear matter properties, selected hyperon optical potentials, and neutron star properties determined for our standard case (for which $\Lambda = 0.9$ GeV, and $R_N^{\rm free} = 1.0$ fm) and the effect of subsequent variations in which differences from the standard parameter set are indicated in column 1. The tabulated quantities at saturation are the slope and curvature of the symmetry energy, L_0 and $K_{\rm sym}$, the incompressibility K_0, skewness coefficient Q_0, calculated at saturation density, and volume component of isospin incompressibility $K_{\tau,v}$, respectively. Tabulated neutron star quantities are the stellar radius, maximum stellar mass, and corresponding central density (units $\rho_0 = 0.16$ fm^{-3}).

Model/ scenario	$g_{\sigma N}$	$g_{\omega N}$	g_ρ	K_0 (MeV)	L_0 (MeV)	$K_{\rm sym}$ (MeV)	Q_0 (MeV)	$K_{\tau,v}$ (MeV)	U_Λ (MeV)	U_{Σ^-} (MeV)	U_{Ξ^-} (MeV)	$M_{\rm max}$ ($M_\odot$)	R (km)	$\rho_c^{\rm max}$ (ρ_0)
Standard	8.97	9.38	4.96	273	84	−23	−305	−431	3	25	5	1.80	11.80	5.88
$\Lambda = 1.0$	9.07	9.73	5.05	278	85	−15	−282	−439	10	32	8	1.84	11.86	5.82
$\Lambda = 1.1$	9.16	10.06	5.16	283	86	−8	−261	−446	16	39	11	1.88	11.94	5.70
$\Lambda = 1.2$	9.24	10.37	5.28	286	87	−2	−241	−451	23	46	15	1.92	12.03	5.60
$\Lambda = 1.3$	9.31	10.67	5.40	289	88	4	−224	−456	29	53	18	1.95	12.10	5.52
$\Lambda = 1.1$, $g_{\sigma Y} \times 1.3$	9.16	10.06	5.16	283	86	−8	−261	−446	−15	14	−4	1.84	11.91	5.78
$\Lambda = 1.3$, $g_{\sigma Y} \times 1.3$	9.31	10.67	5.40	289	88	4	−224	−456	−3	28	3	1.92	12.01	5.66
$\Lambda = 2.0$, $g_{\sigma Y} \times 1.9$	9.69	12.27	6.16	302	92	31	−137	−478	−29	20	−7	2.07	12.24	5.38
Increased $f_{\rho N}/g_{\rho N}$	8.70	9.27	3.86	267	81	−34	−321	−424	6	27	6	1.77	11.61	6.14
Fock $\delta\sigma$	9.01	9.44	4.97	273	84	−21	−296	−432	4	26	5	1.81	11.82	5.86
Eff. Proton Mass	10.40	11.0	4.55	297	101	64	−190	−476	11	41	10	1.94	12.20	5.48
Eff. Proton Mass, $\Lambda = 1.1$	11.08	12.31	4.85	311	111	126	−87	−509	34	67	22	2.07	12.57	5.08
Eff. Proton Mass + $\delta\sigma$	10.89	11.55	4.53	285	109	132	−232	−432	17	49	13	1.99	12.22	5.46
Dirac Only	10.10	9.22	7.84	294	85	0	−299	−424	−23	4	−8	1.79	12.33	5.22
Hartree Only	10.25	7.95	8.40	283	88	−17	−455	−405	−49	−23	−21	1.54	11.73	6.04
Nucleon Only	8.97	9.38	4.96	273	84	−23	−305	−431	3	25	5	2.10	11.08	6.46
$R = 0.8$	9.30	9.85	4.98	277	85	−15	−269	−443	6	25	5	1.83	11.88	5.80
App. $S_0 = 32.5$	9.05	9.38	4.86	275	82	−27	−303	−429	2	24	4	1.80	11.82	5.82
App. $S_0 = 30.0$	9.31	9.35	4.50	280	74	−24	−298	−391	−4	19	1	1.81	11.82	5.76
$S_0 = 30.0$	9.24	9.36	4.61	278	76	−20	−299	−394	−2	21	2	1.81	11.81	5.80

to 10 GeV per nucleon, was modeled as consisting of stable and excited nucleons (Δ and N^*) as well as pions. The basic constraints on this matter are charge symmetry and strangeness conservation (although in this case the strangeness is zero). This is in contrast to matter in cold neutron stars, constrained by charge neutrality and generalized β equilibrium, where strangeness will not be conserved.

The transport theory was extrapolated to cold symmetric and pure neutron matter, with the latter augmented by empirical symmetry pressure [41]. We show in Fig. 3 the pressure versus density for SNM and PNM, as predicted in different scenarios the QMC model in this work. The standard QMC model is consistent with the suggested constraints but at the upper end of the range determined in Ref. [41].

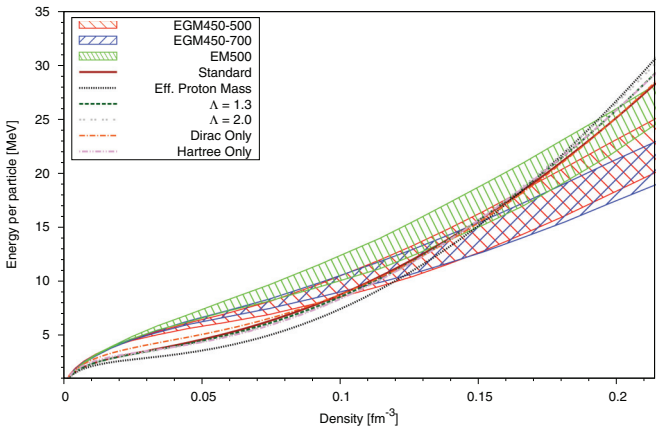

FIG. 1. (Color online) Pure neutron-matter energy per particle as a function of density as obtained in the present work, in comparison with complete CEFT at N^{3}LO order. For more details of the latter, see Ref. [35].

C. Asymmetric nuclear matter

Our knowledge of asymmetric nuclear matter is rather limited, mainly because of a still inadequate understanding of the symmetry energy which describes the response of forces acting in a nuclear system with an excess of protons and neutrons. This is an important property of highly asymmetric systems, such as heavy nuclei and the nuclear matter found in neutron stars, and is defined as

$$\mathcal{S}(\rho) = \frac{1}{2}\frac{\partial^2 E}{\partial \beta^2}\bigg|_{\rho,\beta=0}, \tag{31}$$

where $\mathcal{S}(\rho)$ is equal to the asymmetry coefficient in the Bethe-Weisacker mass formula in the limit $A \to \infty$ [42].

The definition of $\mathcal{S}(\rho)$ in Eq. (31) is related but not identical to the commonly used approximation as the difference between the binding energy per baryon in PNM and SNM,

$$S(\rho) = \mathcal{E}(\rho,\beta = 1) - \mathcal{E}(\rho,\beta = 0), \tag{32}$$

where the binding energy per baryon is

$$\mathcal{E} = \frac{1}{\rho}\left(\epsilon_{\rm hadronic} - \sum_B M_B \rho_B\right). \tag{33}$$

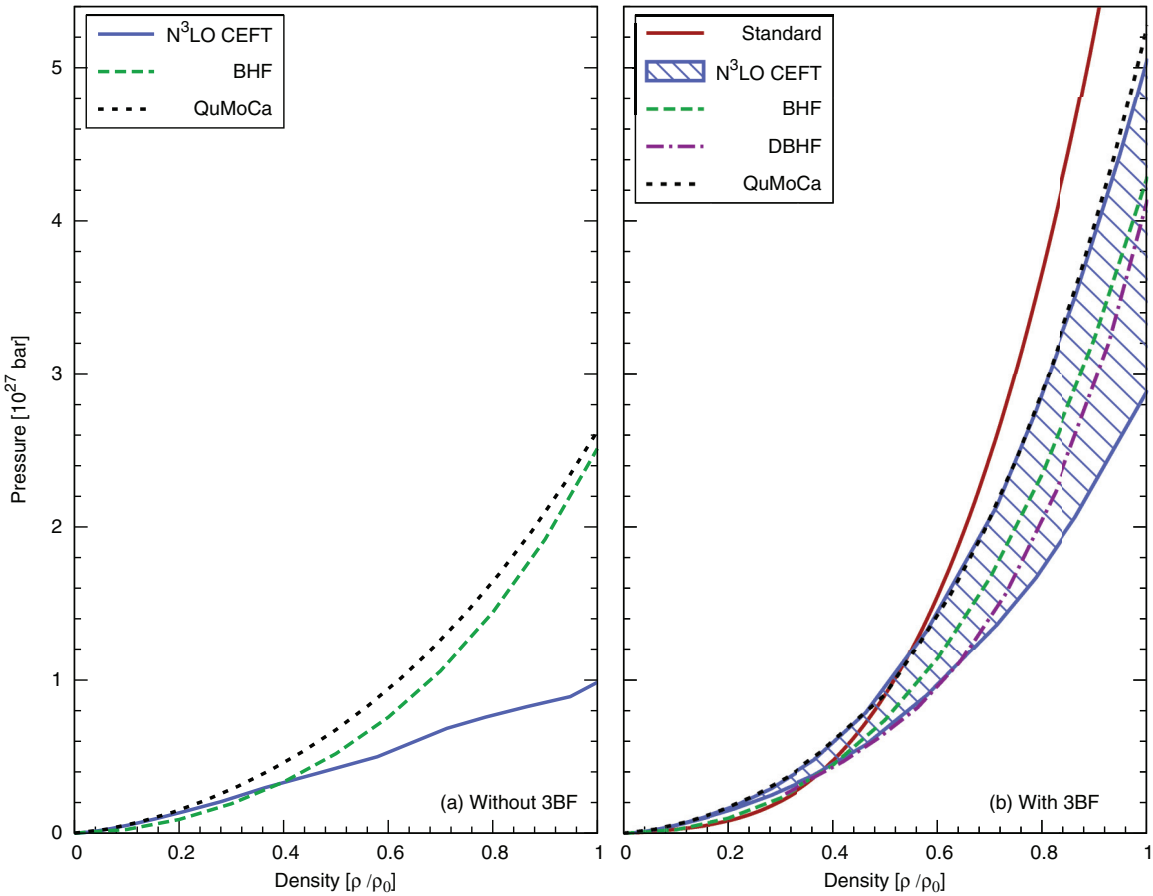

FIG. 2. (Color online) Density dependence of pressure in PNM as predicted in BHF, DBHF, QuMoCa, and CEFT with and without three-body forces: (a) without three-body forces; (b) with three-body forces. The QMC model prediction is shown in (b). For more details, see the text and Ref. [38].

This difference approximation is valid under two assumptions: (i) $E(\rho,\beta = 0)$ is a minimum energy of the matter at a given density ρ and thus in the expansion of $E(\rho,\beta)$ about this value with respect to β the leading nonzero term is the second derivative term and (ii) all the other derivatives in the expansion are negligible [43]. In this work we consider Eq. (32) only to examine the validity of this approximation and to observe the impact of the Fock terms, specifically the tensor contribution, upon the symmetry energy.

The density dependence of the symmetry energy can be expanded about its value at saturation $\mathcal{S}_0$ in terms of the slope L_0, curvature $K_{\rm sym}$, and skewness $Q_{\rm sym}$ (all evaluated at saturation density) as

$$\mathcal{S} = \mathcal{S}_0 + L_0 x + \tfrac{1}{2} K_{\rm sym} x^2 + \tfrac{1}{6} Q_{\rm sym} x^3 + \mathcal{O}(x^4), \qquad (34)$$

where

$$L(\rho) = 3\rho \left(\frac{\partial \mathcal{S}}{\partial \rho}\right), \quad L_0 \equiv L(\rho_{\rm o}),$$
$$K_{\rm sym} = 9\rho_{\rm o}^2 \left(\frac{\partial^2 \mathcal{S}}{\partial \rho^2}\right)_{\rho=\rho_0},$$
$$Q_{\rm sym} = 27\rho_{\rm o}^3 \left(\frac{\partial^3 \mathcal{S}}{\partial \rho^3}\right)_{\rho=\rho_0}. \qquad (35)$$

We note that the curvature of the symmetry energy, $\mathcal{S}$, at saturation density in symmetric matter, is called here $K_{\rm sym}$, the symmetry incompressibility. It should not be confused with K_τ, which is the isospin incompressibility, defined in asymmetric nuclear matter (ANM) by Eq. (38).

The search for constraints on the symmetry energy and its slope, L_0, has received considerable attention during the past decade. Recently, Tsang *et al.* [38] evaluated constraints from a wide range of experiments. However, as again the symmetry energy is not measured directly but extracted from experimental data in a model-dependent way, only limits on the symmetry energy can be established. One of the outcomes of the evaluation was a confirmation of a previously observed correlation between the value of $\mathcal{S}_0$ and its derivative L_0 at saturation density. Taking this correlation into account, the constraint centered on $(\mathcal{S}_0, L_0) \sim$(32.5, 70) MeV, with the uncertainty in $\mathcal{S}_0$ allowing values $30 < \mathcal{S}_0 < 35$ MeV and related values of L_0 in the range of $35 < L_0 < 115$ MeV (see Fig. 2 in Ref. [38] for more details).

While theoretical predictions of $\mathcal{S}_0$ are also more or less confined to the range 30 to 35 MeV, the calculated values of L_0, corresponding to the range of $\mathcal{S}_0$, vary widely. For example, the QuMoCa and CEFT models predict very similar low values of L_0, between ∼30 and 50 MeV [38]. The best performing Skyrme forces, selected in Ref. [10], produce values of L_0

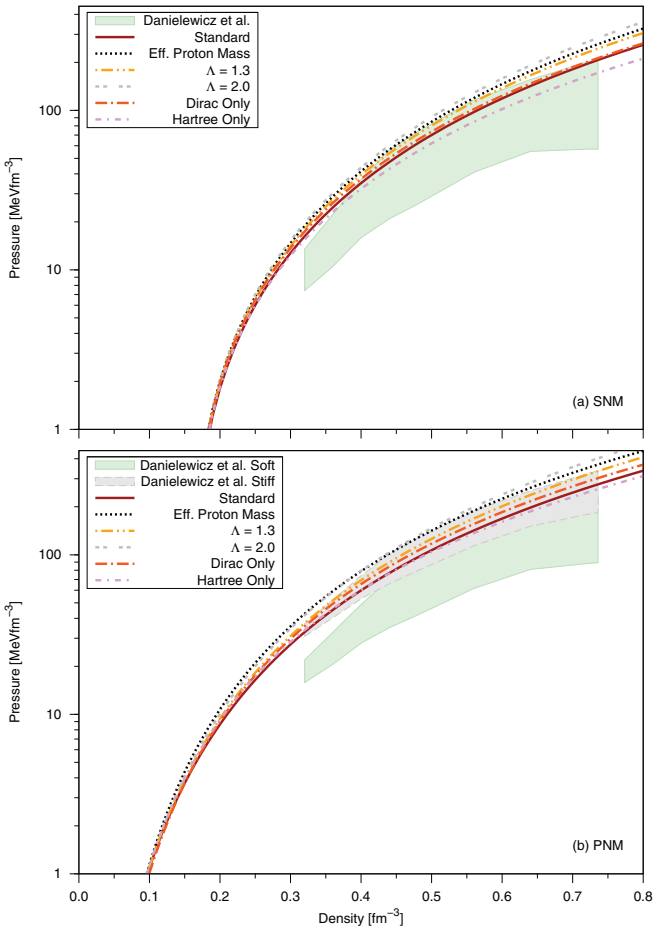

FIG. 3. (Color online) (a) Pressure in SNM as a function of density as predicted in the QMC model. The shaded area is taken from Ref. [41]. (b) Pressure in PNM as a function of density as predicted in the QMC model. The upper and lower shaded areas correspond to two different estimates of the contribution of the symmetry pressure to the total pressure. For more detail, see Ref. [41].

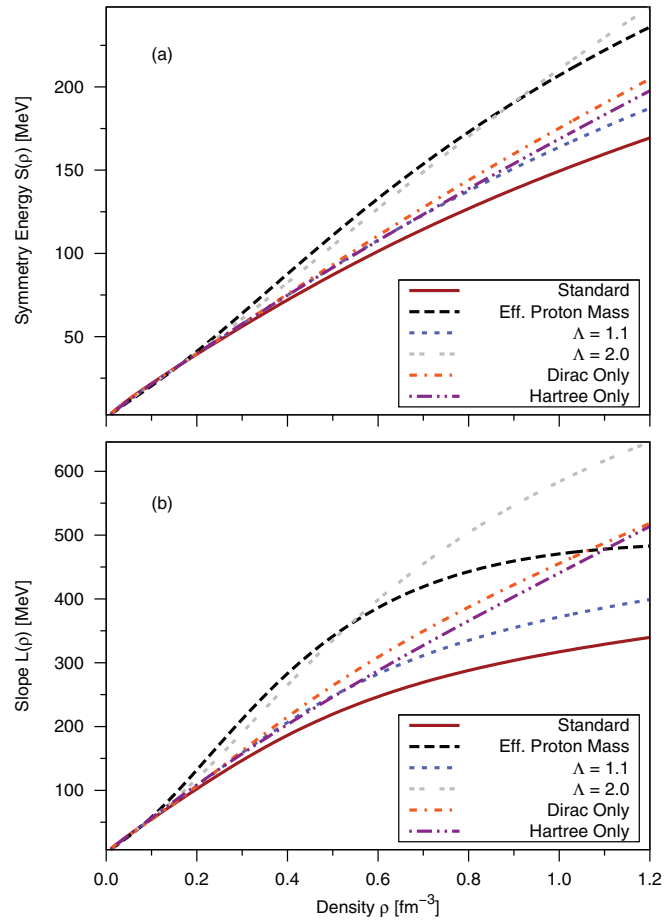

FIG. 4. (Color online) (a) Symmetry energy $\mathcal{S}$ as a function of baryon number density, as calculated in this work. (b) Slope L of the symmetry energy, as a function of baryon number density $L(\rho) = 3\rho(\frac{\partial \mathcal{S}}{\partial \rho})$.

clustered around 50 MeV. However, relativistic mean-field models show a much larger spread. The models which satisfied most of the constraints on the properties of nuclear matter, studied by Dutra *et al.* [44], predicted L_0 in the range ∼50–70 MeV. However, frequently used relativistic mean-field model parametrizations, e.g., NL3, NL-SH, NLC, TM1, and TM2, predict L_0 values of order ∼110–120 MeV [45]. Chen *et al.* [46] found a linear the correlation between $K_{\rm sym}$ and L_0 for a specific selection of equations of state. For a range of positive values of L_0 between about 30 and 120 MeV $K_{\rm sym}$ is between ∼−200 and 100 MeV.

In the QMC model the isospin-dependent part of the interaction is mostly controlled by the exchange of the ρ meson. For this reason, here and in other works (e.g., Ref. [42]) the symmetry energy at saturation $\mathcal{S}_0 = 32.5$ MeV is used to fix the ρ meson coupling constant. The QMC result for L_0 is 84 MeV (see Table II), which is within the broader limits found by Tsang *et al.* [38], although outside their preferred range.

We show the density dependence of the symmetry energy $\mathcal{S}$ and its slope, L, in Fig. 4 and the correlation between $\mathcal{S}_0$ and L_0 in Fig. 5. It can be seen that the linear relationship between $\mathcal{S}_0$ and L_0, observed in QuMoCa calculations [40] and CEFT models [38], is also predicted in this work, although at higher values of L_0 and a somewhat different incline. When the approximate expression is used to evaluate the symmetry energy the linear relationship between $\mathcal{S}_0$ and L_0 is shifted to values which are at most only a few MeV lower.

Another manifestation of isospin asymmetry in nuclear matter can be studied in GMR experiments [33]. The incompressibility of a finite nucleus is obtained, using sum-rule arguments, from the measured energy $E_{\rm GMR}$ in spherical nuclei [31] as

$$K(A,\beta) = M < R^2 > E^2_{\rm GMR}. \tag{36}$$

Here, M is the nucleon mass and R is the rms *matter* radius of the nucleus with mass number A. $K(A,\beta)$ can be expressed in a form of an expansion in terms of $A^{-1/3}$ and β [31],

$$K(A,\beta) = K_{\rm vol} + K_{\rm surf}A^{-1/3} + K_{\rm curv}A^{-2/3} + K_\tau\beta^2 + K_{\rm coul}\frac{Z^2}{A^{4/3}} + \cdots, \tag{37}$$

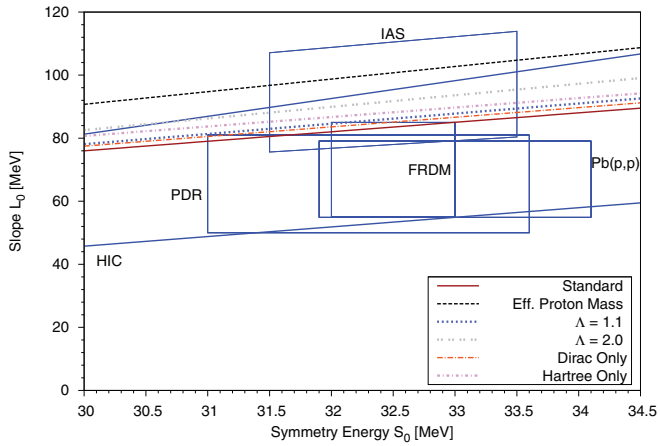

FIG. 5. (Color online) The correlation between the slope and magnitude of the symmetry energy $\mathcal{S}_0$. Constraints on the slope L_0 and the symmetry energy S_0 at saturation density from different experiments are overlayed. The experimental methods are labeled next to the boxes with the estimated uncertainties. See Ref. [38] for more details.

where the symmetry-related coefficient consists of the volume and surface components [31,47,48],

$$K_\tau = K_{\tau,v} + K_{\tau,s} A^{-1/3}, \tag{38}$$

with $K_{\tau,\mathrm{v}}$ ($K_{\tau,s}$) the volume (surface) symmetry incompressibility.

The coefficient $K_{\tau,v}$ can be evaluated using

$$K_{\tau,v} = \left(K_{\mathrm{sym}} - 6L_0 - \frac{Q_0}{K_0} L_0 \right). \tag{39}$$

Stone *et al.* [33] analyzed all currently available GMR data in nuclei with $56 < A < 208$ and found a limit $-700 \leqslant K_{\tau,v} \leqslant -372$ MeV. The QMC result is $K_{\tau,v} = -431$ MeV, which lies well within the experimental limits.

D. Generalized β equilibrium matter and neutron stars

In this section we study cold ANM which is expected to exist in the outer core of cold neutron stars.

Dense matter just above the saturation density, when all nuclei are dissolved, forms a system of interacting nucleons and leptons. If this form of matter exists long enough on the time scale of weak interactions, $\tau \approx 10^{-10}$ s, BEM develops between β decay $n \to p + e^- + \tilde{\nu}$ and its inverse. When the density increases to about 2–3ρ_0 and because baryons obey the Pauli principle, it becomes energetically favorable for nucleons at the top of the corresponding Fermi sea to convert to other baryons. A GBEM develops with respect to all reactions involving either weak or strong interactions, which lead to the lowest-energy state. Only two quantities are conserved in GBEM: the total charge (zero in stars) and total baryon number. Strangeness is conserved only on the time scale of strong interaction, $\tau \approx 10^{-24}$ s, and lepton number is conserved only on the time scale of tens of seconds, because of the diffusion of neutrinos out of the star [42].

To describe GBEM, it is convenient to use the chemical potentials of the participating particles. It can be shown that there are as many independent chemical potentials as the number of conserved quantities. Thus, we need to choose just two, for example, the chemical potentials of the neutron and electron. Chemical potentials of all the other species in GBEM are then expressed via a relation

$$\mu_i = B_i \mu_n - Q_i \mu_e, \tag{40}$$

where the baryon number, B, is 0 or 1 and the charge number, Q_i, is 0 or ± 1. Alternatively (and equivalently), the chemical potentials can be related to Lagrange multipliers [as the degrees of freedom for charge conservation (ν) and baryon number conservation (λ)] to solve a system of equations,

$$0 = \mu_i + B_i \lambda + \nu Q_i, \tag{41}$$

$$0 = \mu_\ell - \nu, \tag{42}$$

$$0 = \sum_i B_i \rho_i - \rho, \tag{43}$$

$$0 = \sum_i B_i \rho_i Q_i + \sum_\ell \rho_\ell Q_\ell, \tag{44}$$

to obtain the number densities for each particle ($i \in \{n, p, \Lambda, \Sigma^-, \Sigma^0, \Sigma^+, \Xi^-, \Xi^0\}$ and $\ell \in \{e^-, \mu^-\}$), ρ_i, as well as the Lagrange multipliers. At the Hartree-Fock level, the following formulas to numerically evaluate the chemical potentials must be used to ensure we encapsulate the Fock contribution to the energy densities correctly:

$$\mu_i = \frac{\partial \epsilon_{\mathrm{total}}}{\partial \rho_i}, \quad \mu_\ell = \frac{\partial \epsilon_\ell}{\partial \rho_\ell} = \sqrt{k^2 + m_\ell^2}. \tag{45}$$

In Figs. 6 and 7 we show the EoS (with various parameter variations) and the distribution of species in GBEM matter for the preferred scenario in this work. We note that the pressure now involves the total energy density (including leptonic contribution) $\epsilon_{\mathrm{total}} = \epsilon_{\mathrm{hadronic}} + \epsilon_\ell$:

$$P_{\mathrm{total}} = \rho^2 \frac{\partial}{\partial \rho} \left(\frac{\epsilon_{\mathrm{total}}}{\rho} \right) = \sum_i \mu_i \rho_i - \epsilon_{\mathrm{total}}. \tag{46}$$

The kinks in pressure in Fig. 6 appear at hyperon thresholds. A comparison between calculations for Hartree alone, Hartree-Fock with only the Dirac piece of the coupling to vector mesons, or the full model highlights the importance of the Fock terms at high density. As compared to the EoS of matter in which the hyperons are not included above their natural thresholds and nucleons are assumed to be the only baryons up to densities ~5–6ρ_0, the pressure in GBEM increases with density more slowly. It is challenging to produce reasonable scenarios where the empirical constraints are met and the pressure still increases fast enough to support high-mass, cold neutron stars, as are discussed in the next section.

In Fig. 7 the particle content of GBEM matter and corresponding Fock energy contributions is displayed for three scenarios, "Standard," "Eff. Proton Mass," and "$\Lambda = 2.0$,

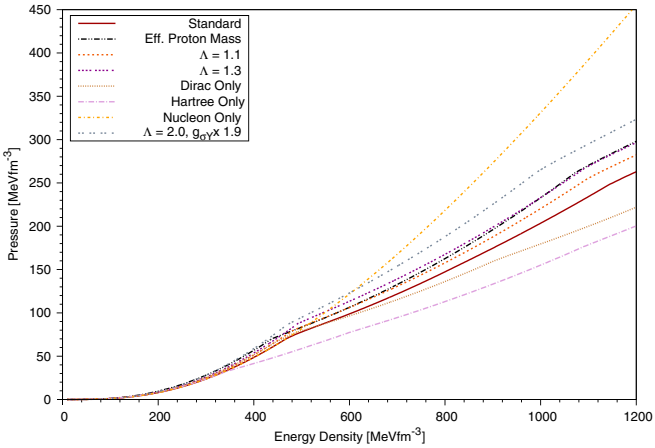

FIG. 6. (Color online) GBEM EoS. Kinks occur at significant hyperon threshold densities. The divergences between the Hartree only QMC parametrization and the Hartree-Fock scenarios highlight the importance of Fock terms at high density. The Nucleon only BEM EoS is added for a comparison.

$g_{\sigma Y} \times 1.9$." In the Standard scenario, the first hyperon to appear is Σ^-, at 0.46 fm^{-3}, followed by Ξ^- at 0.47 fm^{-3}. The Σ^- is quickly replaced with the Ξ^-, which is then followed by the appearance of Λ at 0.74 fm^{-3} and then Ξ^0 at 0.97 fm^{-3}. Because the latter is above the maximum density reached in any of our realistic model variations, it is largely irrelevant. We show in Fig. 8 that the Λ chemical potential approaches and meets the neutron chemical potential, meaning that it is energetically favorable for it to appear. However, for the Σ^- we see that at low density it is more favorable than the Ξ^-, while beyond $\sim$0.4 fm^{-3} this is no longer so.

Once the full Fock terms are included, the results for the standard scenario are no longer consistent with the known values of the phenomenological hyperon optical potentials. This is because of a change in the ratio of the scalar to vector coupling, effectively leaving the Λ hyperon unbound. The additional attraction generated by the Fock terms, especially the ρ tensor contribution, has altered the coupling constants such that the ω coupling is larger. This effect of an increase in the vector coupling is illustrated by the larger maximum neutron star masses, which also correspond to poor results for the hyperon optical potentials.

In the work of Miyatsu *et al.* the scalar couplings from the QMC model were not used. Instead, they rescaled the scalar coupling of each hyperon to obtain an acceptable optical potential. We consider the possibility of rescaling the scalar coupling reasonable, as the bag model used is a very simple model of the baryons in which only the light quarks participate in the interaction. An amplification of only the hyperon scalar couplings of 30% is considered in "$\Lambda = (1.1, 1.3)$, $g_{\sigma Y} \times 1.3$." This improves the predictions of the optical potentials, binds the Λ hyperon, and maintains a repulsive potential for the Σ^- hyperon. In doing this the optical potentials are closer to the values extracted from experimental studies of hypernuclei, but the EoS of β-equilibrated matter is much softer; Λ and Σ^- both appear. In the scenario "$\Lambda = 2.0$, $g_{\sigma Y} \times 1.9$," we meet both the constraints of phenomenological hyperon optical potentials and high-mass neutron star observations. In this scenario we increase the form factor cutoff and hence the strength of the Fock terms forcing the vector coupling to become larger

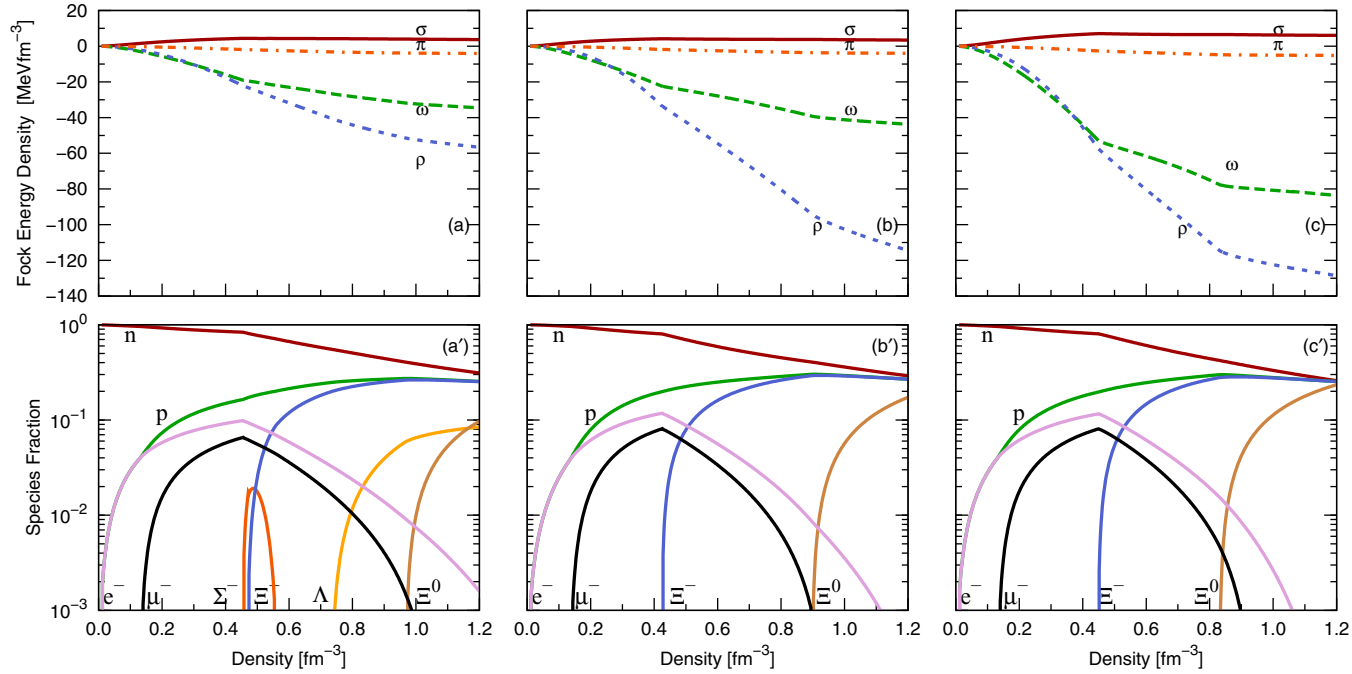

FIG. 7. (Color online) (Top) Fock energy-density contributions and (bottom) species fraction as a function of baryon number density in GBEM, for the Standard (a,a′), Eff. Proton Mass (b,b′), and the $\Lambda = 2.0$, $g_{\sigma Y} \times 1.9$ (c,c′) scenarios. The corresponding EoSs are shown in Fig. 6.

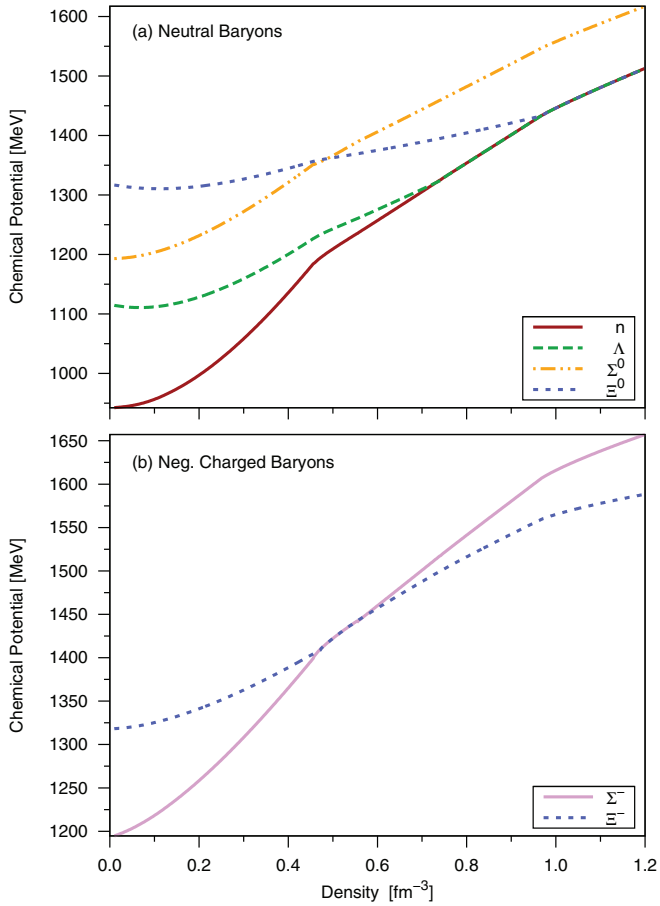

FIG. 8. (Color online) (a) Neutral baryon chemical potentials as a function of baryon number density for the standard scenario. (b) Negative-charge baryon chemical potentials as a function of baryon number density for the standard scenario.

and then rescale the hyperon scalar coupling. In this very phenomenological scenario we obtain reasonable values for the optical potentials and still obtain high-mass neutron stars.

In the scenario Eff. Proton Mass the ratio of tensor to vector coupling is rescaled using the effective proton mass in Eq. (14), as opposed to the free proton mass. This is a naive way to introduce a scalar dependence into the Pauli term coupling. This substitution effectively increases the strength of the Pauli term owing to the reduction of the proton mass. The change in strength of the tensor coupling has a significant impact on the composition. Its impact on the results for neutron stars is discussed in the Secs. III F and III E. This particle content is different from our standard scenario and most other models, which generally find that either the Λ or the Σ^- appears first. The increased strength of the tensor contribution, and hence attraction, has increased the vector coupling and as a consequence the Λ is not bound at saturation density in SNM. This combined with the attraction from the Fock terms for the Ξ's makes them more energetically favorable than Λ or the Σ^-.

At the Hartree level the "hyperfine" interaction from OGE makes the Λ more energetically favorable than the Σ^-, providing a source of attraction for the former and repulsion for the latter. This has been shown at the Hartree level in the QMC model to suppress the appearance of Σ^- hyperons in GBEM matter [49]. This can also be considered a qualitative explanation for the absence of medium to heavy Σ hypernuclei [15].

We consider the extreme scenario $\Lambda = 2.0$, $g_{\sigma Y} \times 1.9$, where we maintain a large vector coupling by increasing the form factor cutoff, effectively increasing the strength of the Fock terms, and we rescale the scalar coupling to obtain reasonable values for the phenomenological hyperon optical potentials, so that the Λ is bound at saturation density in symmetric nuclear matter. Even though the Λ feels a significant attraction at saturation density, it appears that it cannot compete with the attraction generated by the Fock terms at high density—specifically the tensor part—for the Ξ. The contributions of the Fock energies is more significant and the composition is similar to Eff. Proton Mass.

E. Cold neutron stars

To calculate neutron star properties, such as the total gravitational mass, $M(R)$, and the baryon number, $A(R)$, within the stellar radius R, we solve the TOV equations [50] for hydrostatic equilibrium of spherically symmetric (nonrotating) matter. Using the EoS calculated here, this is self-supported against gravitational collapse:

$$M(R) = \int_0^R 4\pi r^2 \epsilon_{\text{total}}\, dr, \tag{47}$$

$$\frac{dP_{\text{total}}}{dr} = -(\epsilon_{\text{total}} + P_{\text{total}})\frac{[M(r) + 4\pi r^3 P_{\text{total}}]}{r^2[1 - 2M(r)/r]}, \tag{48}$$

$$\frac{dA}{dr} = \frac{4\pi r^2 \rho}{\sqrt{1 - 2M(r)/r}}. \tag{49}$$

In Eqs. (47)–(49) we use units in which $G = 1$. The difference between the total gravitational mass and baryonic mass within a radius R is defined by $M(R) - A(R)M_N$.

The EoS of GBEM is not valid in the outer regions (crust) of the star, where nuclei and nuclear processes become dominant. Following the customary procedure, we introduce a smooth transition between our EoS in GBEM and the standard low-density EoS of Baym, Pethick, and Sutherland (BPS) [51] at low density.

The relationship between stellar mass and radius, obtained as the solution of the TOV equations, Eqs. (47) and (49), is summarized in Table II and depicted in Fig. 9. We find that the predicted maximum masses for several of the scenarios, lie very close to the constraints set by Demorest *et al.* [52] of a $(1.97 \pm 0.04)M_\odot$ pulsar, as well as the new constraint set by PSR J0348 + 0432 with a mass of $2.03 \pm 0.03 M_\odot$ [53]. The corresponding radii are somewhat larger than that extracted from recent observations of Type I x-ray bursters (see, e.g., Refs. [54,55]). Extraction of radii from observation is rather complicated and there are still many questions to be addressed. For example, Steiner *et al.* [54] analyzed observations of six low-mass x-ray binaries (emitting x rays regularly) and their statistical analysis yielded R in the range 10–12 km for masses around $1.6M_\odot$. However, the uncertainty in the

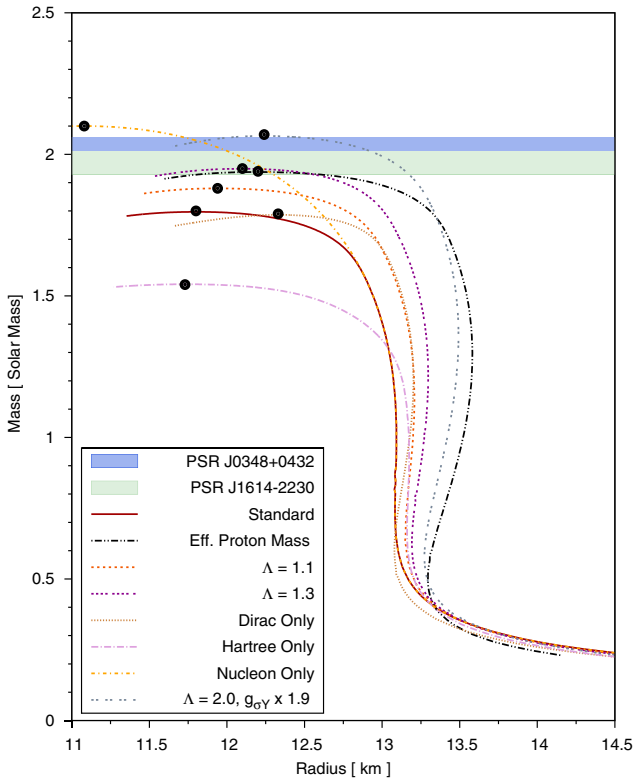

FIG. 9. (Color online) Gravitational mass versus radius relationship for various scenarios described in the text. The black dots represent maximum-mass stars and the colored bars represent observed pulsar constraints.

relation between the extracted photospheric radius and the actual radius of the star remains large. The results of Guillot *et al.*, namely, $R = 9.1^{+1.3}_{-1.5}$ km (90% confidence), are based on observations of five quiescent low-mass x-ray binaries (which emit x rays only occasionally) under the assumption that the radius is constant for a wide range of masses.

While the observations Refs. [52,53] provide constraints on high-mass neutron stars, the observation of the double pulsar J0737-3039 and its interpretation [56] offers a constraint on the neutron star EoS in a region of central densities $\sim$2–3ρ_0. The constraint concerns the ratio between the gravitational and baryonic mass of the star. The gravitational mass of pulsar B is measured very precisely to be $M_g = 1.249 \pm 0.001 M_\odot$ and the baryonic mass depends on the mode of its creation, which can be modeled. If pulsar B was formed from a white dwarf with an O-Ne-Mg core in an electron capture supernova, with no or negligible loss of baryonic mass during the collapse, the newly born pulsar should have the same baryonic mass as the progenitor star. Podsiadlowski *et al.* [56] estimated the baryonic mass of the pulsar B to be between 1.366 and $1.375 M_\odot$. Another simulation of the same process, by Kitaura *et al.* [57], gave a value for the baryonic mass of $1.360 \pm 0.002 M_\odot$. We show in Fig. 10 the QMC result, which supports the model of Kitaura *et al.*, accepting some small loss of baryonic mass during the birth of pulsar B.

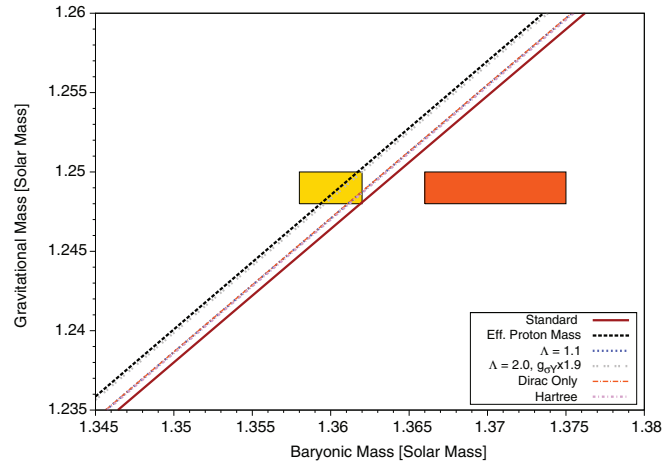

FIG. 10. (Color online) Gravitational mass versus baryonic mass. The boxes are constraints from simulations (yellow) by Kitaura *et al.* [57] and (orange) by Podsiadlowski *et al.* [56], which are explained in the text.

F. Sensitivity to parameter variation

Our calculations for the Hartre-Fock QMC model follow lines similar to those in Refs. [18–20] in that in each case an approximation is made for the Fock terms. More specifically, in our calculation of the Fock terms we omit energy transfer in the meson propagator (meson retardation effects). We also omit the modification of momenta because of the vector component of the self-energy, which has been shown to be small in Refs. [20] and [21]. We include the tensor interaction in the Fock terms, with a common form factor, which has a dipole form. The lowest mass, Λ, for that cutoff, which should be larger than the masses of the mesons included, is 0.9 GeV. This is taken as our standard or baseline scenario value for two reasons.

(i) The incompressibility K_0 rises as Λ is increased. In the range $\Lambda = 0.9$–2.0 GeV, for the scenarios considered K_0 remains within the range $250 \leqslant K_0 \leqslant 315$ MeV, which was the constraint derived in Ref. [33].

(ii) Increasing the form factor cutoff Λ effectively increases the strength of the Fock terms, for which the ω and ρ mesons contribute a significant attraction once contact subtraction has been performed. To obtain the saturation properties of SNM, one must compensate for this additional attraction, resulting in a larger vector coupling. If the vector couplings of the hyperons are simply related to to the vector couplings of the nucleons by Eq. (25), the results for the hyperon optical potentials at saturation density in SNM are not consistent with the values extracted from hypernuclear experiments largely because of the change in the ratio of the scalar to vector couplings.

We demonstrate the effect of changing the value of Λ between 0.9 and 1.3 GeV in the subsequent scenarios (lines 2–5) in Table II, which differ from the standard one only by the value of Λ. We observe a minor increase in K_0 and L_0,

which both remain within the empirical expected range and an increase in the maximum mass the the neutron star by ∼8%.

However, once the full Fock terms are included, the results for the standard scenario, even with variable Λ, are not consistent with values of the phenomenological hyperon optical potentials extracted from experiments. This is because of a change in the ratio of the scalar to vector coupling, leaving effectively the Λ hyperon unbound. The additional attraction generated by the Fock terms, especially the ρ tensor contribution, has altered the coupling constants such that the ω coupling is larger.

In the extreme scenario $\Lambda = 2.0$, $g_{\sigma Y} \times 1.9$ discussed in Sec. III D, we meet both the constraints of phenomenological hyperon optical potentials and high-mass neutron star observations.

In the scenarios Eff. Proton Mass, Eff. Proton Mass, $\Lambda =$ 1.1, and Eff. Proton Mass + $\delta\sigma$ (lines 11–13 of Table II) the ratio of tensor to vector coupling is rescaled using the effective proton mass in Eq. (14) as opposed to the free proton mass. This is a simplified way to introduce a scalar dependence into the Pauli term coupling. This substitution effectively increases the strength of the Pauli term owing to the reduction of the proton mass. The change in strength of the tensor coupling has a significant impact on the composition. It causes a significant increase in K_0 as Λ takes on larger values. Indeed, as we see in Table II, K_0 rises above 311 MeV for Λ greater than 1.1 GeV. Similar observations apply for the slope of the symmetry energy at saturation density, L_0. Because of the increased vector coupling, the maximum mass of the neutron star is significantly increased, but the hyperon optical potentials remain at variance with expected values.

The contribution to the mean scalar field arising from the Fock terms is incorporated in the cases denoted Fock $\delta\bar{\sigma}$ and Eff. Proton Mass + $\delta\sigma$. When applied to neutron star properties it negligibly increases the maximum mass in our baseline scenario and increases it by a few percent when a scalar dependence is introduced into the Pauli term to just below $2M_\odot$.

The tensor couplings used in this work, arising from the underlying MIT bag model, are consistent with vector meson dominance (VDM) and hence our tensor couplings are calculated from the experimental magnetic moments. Purely as a test of the effect of a variation in those couplings we arbitrarily took the ratios of tensor to vector couplings of all baryons from the Nijmegen potentials (Table VII of Ref. [30]), where there is a larger value of $f_{\rho N}/g_{\rho N} = 5.7$. These were also used by Miyatsu *et al.* [21,26]. This variation, denoted Increased $f_{\rho N}/g_{\rho N}$, produced an EoS for GBEM, which was indistinguishable from our standard result.

In the scenarios Dirac only, Hartree only, and Nucleon only, we show results of the QMC calculation with the same parameters as the standard set but leaving out the Pauli part of the Fock term, the full Fock term, and the hyperons, respectively. These results are particularly useful for understanding of the role of individual terms in the QMC Lagrangian.

The last four scenarios in Table II document the effect of changes in the value of the free nucleon radius and the evaluation of the symmetry energy from the difference formula Eq. (32) App. and from the second derivative the the energy per particle $S_0 = 30.0$. Neither effect changes significantly the properties of GBEM matter and neutron stars.

G. Comparison with other models

The Hartree-Fock calculation in Ref. [24] differs considerably from that presented here, as well as from that in Refs. [21,26,58,59]. The first and major difference is that the tensor interaction of the baryons is ignored, whereas in Refs. [21,26,58,59] and in our work it is found to have a very significant effect. A second difference among Ref. [24], our work, and Refs. [21,26,58,59] is that in their preferred QMC scenario (QMC-HF3) they artificially adjust a parameter, C, which is related to the scalar polarizability, to obtain a lower value for the incompressibility. This represents a dramatic change in the model.

The masses of the baryons in the QMC model are determined by the bag equations and the scalar coupling is calculated directly from the density dependence of the baryon mass in medium. Thus, changing C, or equivalently the scalar polarizability, changes the mass and the density-dependent coupling in a manner which is inconsistent with the traditional form of the QMC model [16]. In this manner, the many-body interaction is also being changed through the density-dependent scalar coupling. Their QMC-HF3 variation gives an incompressibility of $K = 285$ MeV and a very low prediction for the maximum mass of neutron stars, $M = 1.66M_\odot$. In our Dirac-only variation we find a slightly larger value for the incompressibility, $K = 294$ MeV with a maximum stellar mass of $M = 1.79M_\odot$. Other variations were considered in Ref. [24], where they do not modify C: one where they calculate fully relativistic Fock terms and another where they make a nonrelativistic approximation to the Fock terms. These variations both produce maximum masses of neutron stars of $M = 1.97M_\odot$.

References [21,26,58,59] carry out a relativistic calculation in which they treat the Fock and Hartree terms on the same level. More precisely they calculate self-energy contributions arising from both terms and these self-energies modify the baryon mass, momentum, and energy. They include the tensor interaction, subtract contact terms, and consider two variations of the bag model. In their first paper [21] they used much larger values for the tensor couplings without form factors. In the later paper [58] they include the effect of form factors, ignoring effects of meson retardation (as we do) but with a lower cutoff mass, i.e., $\Lambda = 0.84$ GeV. The latter had the effect of keeping the incompressibility from being too large. Their conclusions are very similar to our own, in that they find that the tensor terms provide a source of attraction and that overall the Fock terms enhance the maximum neutron star mass.

The maximum stellar masses in their first paper [21] are larger than those in their second paper [58], almost certainly because the inclusion of the form factor decreases the effect of the Fock term at high density. They consider two variations of the QMC model: one with, and one without the pion contribution in the bag (CQMC), which tends to give a slightly stiffer EoS, because of its effect on the baryon masses. For QMC they obtain $M = 1.86M_\odot$, $R = 11.2$ km, and for

CQMC $M = 1.93M_{\odot}$, $R = 11.5$ km for the maximum stellar mass solutions. Despite the differences in how we handle the Fock terms and their use of larger tensor couplings and more phenomenological hyperon couplings, we are led to the same conclusions about the importance of the tensor contribution. We also find a very similar particle content in scenarios where the Fock terms are quite strong, such as the Eff. Proton Mass and $\Lambda = 2.0$, $g_{\sigma Y} \times 1.9$ scenarios, where the Ξ^- is the first hyperon to appear.

IV. DISCUSSION

To treat the EoS of matter at the densities typical of neutron stars one must treat the motion of the baryons relativistically. The QMC model not only does that but it self-consistently treats the in-medium changes in baryon structure induced by the large scalar mean fields generated in such matter. As we have explained, those changes, which may be represented by the corresponding scalar polarizabilities, lead naturally to predictions for the three-body forces between not just the nucleons but the nucleons and hyperons as well as hyperons, without additional parameters. This widely used approach has been extended here to include the effect of Fock terms arising from the tensor (or Pauli) couplings of the baryons to vector mesons, especially the ρ.

The results for a comprehensive set of nuclear matter properties, including K_0, L_0, $K_{\rm sym}$, Q_0, and $K_{\tau,v}$ have been studied in detail. The model prediction for the incompressibility lies within the range extracted from experimental data for most model variations considered. While the incompressibility is increased by this addition in some cases and tends to lie at the mid to top end of the acceptable range, it serves as a useful constraint on the additional mass parameter, Λ, associated with the form factor that appears at the meson-baryon vertices (the latter only being needed when the Fock terms are computed). The modest variation of the nuclear matter observables with this parameter (which must lie above the masses of the exchanged mesons included in the theory) is illustrated in Table II. Increasing Λ beyond 0.9 GeV raises the incompressibility and in the case denoted Eff. Proton Mass, $\Lambda = 1.1$ GeV it is close to the limit $K_0 < 315$ MeV.

The symmetry energy and its slope are noticeably influenced by the Fock terms; specifically, curvature is introduced into these quantities through the tensor interaction, as can be seen in Fig. 4. At saturation density we find in all cases that the isospin incompressibility is within accepted constraint limits and while the slope of the symmetry energy is on the larger side, it does lie within the broad limits reported by Tsang *et al.* [38].

It is interesting to note that there is a satisfying level of consistency between theoretical predictions of N^{3}LO chiral effective field theory and the QMC model results studied here for densities of PNM up to and around nuclear matter density. Above saturation density a slightly higher energy per particle as a function of density is found here. It is also found that the natural incorporation of many-body forces in the QMC model tends to produce a somewhat stiffer PNM EoS above saturation density than other models including three-body forces.

Even at densities above three times nuclear matter density, the nucleon Fock terms are found to contribute significantly to the EoS and the corresponding attraction is what is responsible for the increased pressure and larger maximum stellar masses in several scenarios. This can be seen in Fig. 9, where there is a clear transition from a Hartree QMC calculation to a Hartree-Fock calculation with no tensor interaction (Dirac-only; no Pauli term), to our Eff. Proton Mass calculation [Dirac and Pauli (with scalar dependence) terms]. In these three variations, and those with increasing form factor mass, Λ, the maximum stellar mass increases because of the increased vector coupling and pressure coming from the Fock terms. This increased pressure arises mainly from the ρ meson contribution. As we can readily see in Table II and Fig. 9, the value of Λ cannot be varied far in the Eff. Proton Mass calculations. Indeed, in that case, the incompressibility is already as high as it can be. The maximum neutron star mass, for our Standard scenario is approximately the same as the Dirac only scenario because of the change in composition, where in the latter the appearance of Σ^- is avoided and only the Λ and Ξ^- followed by the Ξ^0 appear. Even with the brief appearance of an additional hyperon in our baseline scenario, the value of $M_{\rm max}$ is still slightly larger because of the tensor interaction. We see that the maximum neutron star mass, for the case of nuclear matter in β equilibrium where hyperons must appear, lies in the range 1.80 to $2.07M_{\odot}$.

The EoS and the maximum masses of the corresponding neutron stars are insensitive to the choice of the larger ρ tensor couplings used, for example, by Miyatsu *et al.* [21]. Similarly, modest variations in the radius of the free nucleon have only very minor effects on these quantities. Finally, we note that the correction ($\delta\bar{\sigma}$) to the scalar mean field arising from the Fock terms has a negligible effect on the incompressibility in our baseline scenario. On inclusion of a naive scalar dependence into the Pauli term it decreases the incompressibility by 12 MeV, yet other observables remain largely unaltered by this addition.

This, plus the dependence of the incompressibility and maximum mass on Λ, leads us to conclude that the Hartree-Fock model used here with only σ, ω, ρ, and π mesons can only reproduce nuclear matter properties, phenomenological hypernuclear optical potentials, and massive neutron star observations if there is significant rescaling of the hyperon coupling constants. Allowing for the rescaling of hyperon couplings, we conclude that the maximum mass allowed in the model lies in the range 1.8–$2.1M_{\odot}$.

It is the treatment of the lightest mesons that is the most important, and the inclusion of heavier mesons would necessarily be more model dependent. For this reason, in this work we have restricted ourselves to just σ, ω, ρ, and π mesons. The model could be extended to include mesons containing strange quarks, of which the next lightest mesons are $K(495)$ and $K^*(895)$. These mesons will induce mixing in the baryon octet, possibly changing the composition of matter in generalized β equilibrium. These mesons will be studied in a future work. Heavier mesons such as the hidden strangeness vector meson $\phi(1020)$ have been considered in other works (Refs. [60,61]), which have found that they can produce extra vector repulsion delaying the onset of hyperons. It should

be noted that with every new meson that is included more parameters must be introduced into the model.

For the matter considered in the present paper we take the view that hadrons remain the relevant degrees of freedom. Transitions to quark matter have been studied by many authors; see Refs. [62–64] for recent accounts. Such a transition may indeed be possible in the interior of neutron stars. We will investigate such a transition in a future work.

We stress that the QMC model does not predict a significant abundance of Σ hyperons at any density where the model can be considered realistic and they are completely absent in model variations compatible with large neutron star mass observations. This is in contrast to a number of other relativistic models which do predict the Σ threshold to occur, even prior to that of the Λ [65,66]. We note that Schaffner-Bielich [65] considered a phenomenological modification of the Σ potential with additional repulsion, which significantly raised its threshold density. In the case of the QMC model the physical explanation of the absence of Σ hyperons is very natural, with the mean scalar field enhancing the repulsive hyperfine force for the in-medium Σ (recall that the hyperfine splitting, which arises from OGE, determines the free Σ-Λ mass splitting in the MIT bag model).

Purely for comparison purposes, we also include a nucleon-only scenario, in which hyperons are artificially excluded. In this case the EoS is increasingly stiffer at densities above 0.4 fm^{-3}, leading to a large maximum stellar mass of $2.10 M_\odot$, consistent with many other nucleon-only models.

It is worth remarking that upon inclusion of the tensor coupling, the proton fraction increases more rapidly as a function of total baryon density. This is likely to increase the probability of the direct Urca cooling process in proto-neutron stars. As a further consequence, the maximum electron chemical potential is increased in this case, which may well influence the production of π^- and $\bar{K}$ condensates. Changes to the Λ threshold (it occurs at higher density with lower maximum species fraction) reduce the possibility of H-dibaryon production as constrained by β-equilibrium of the chemical potentials.

In summary, taking into account the full tensor structure of the vector-meson-baryon couplings in a Hartree-Fock treatment of the QMC model results in increased pressure at high density—largely because of the ρN tensor coupling—while maintaining reasonable values of the incompressibility at saturation density. The conceptual separation between the incompressibility at saturation density and the slope of the symmetry energy or "stiffness" at higher densities is critical. It is the latter that leads to neutron stars with maximum masses ranging from $1.8 M_\odot$ to $2.1 M_\odot$, even when allowance is made for the appearance of hyperons. This suggests that hyperons are very likely to play a vital role as constituents of neutron stars with central densities above three times nuclear matter density.

ACKNOWLEDGMENTS

J.R.S. is pleased to acknowledge the hospitality of the CSSM at the University of Adelaide, where this work was carried out. We thank Kai Hebeler for providing numerical data for the CEFT results in Fig. 1. This work was supported by the University of Adelaide and the Australian Research Council through Grant No. FL0992247 (A.W.T.) and through the ARC Centre of Excellence for Particle Physics at the Terascale. D.L.W. was supported by an ARC postgraduate scholarship. The work of K.T. was supported by the Brazilian Ministry of Science, Technology and Innovation (MCTI-Brazil) and Conselho Nacional de Desenvolvimento Científico e Tecnológico (CNPq), Project No. 550026/2011-8.

APPENDIX

The integrands take the following form for $B = B'$:

$$\Xi_B^\sigma = \frac{1}{2}\frac{[g_{\sigma B} C_B(\bar{\sigma}) F^\sigma(\mathbf{k}^2)]^2}{E^*(\mathbf{p}')E^*(\mathbf{p})} \times \left\{M_B^{*2} + E^*(\mathbf{p}')E^*(\mathbf{p}) - \mathbf{p}'\cdot\mathbf{p}\right\}\Delta_\sigma(\mathbf{k}). \quad \text{(A1)}$$

Here for the vector meson integrands we denote $\eta = \omega, \rho$,

$$\Xi_B^{\eta V} = -\frac{\left[g_{\eta B} F_1^\eta(\mathbf{k}^2)\right]^2}{E^*(\mathbf{p}')E^*(\mathbf{p})} \times \left\{2M_B^{*2} - E^*(\mathbf{p}')E^*(\mathbf{p}) + \mathbf{p}'\cdot\mathbf{p}\right\}\Delta_\eta(\mathbf{k}), \quad \text{(A2)}$$

$$\Xi_B^{\eta VT} = (g_{\eta B})^2 \kappa_{\eta B} F_1^\eta(\mathbf{k}^2) F_2^\eta(\mathbf{k}^2) \cdot\left\{\frac{-3M_B^{*2} + 3E^*(\mathbf{p}')E^*(\mathbf{p}) - 3\mathbf{p}'\cdot\mathbf{p}}{E^*(\mathbf{p}')E^*(\mathbf{p})}\right\}\Delta_\eta(\mathbf{k}), \quad \text{(A3)}$$

$$\Xi_B^{\eta T} = -\frac{\left[g_{\eta B}\kappa_{\eta B} F_2^\eta(\mathbf{k}^2)\right]^2}{E^*(\mathbf{p}')E^*(\mathbf{p})} \cdot\left\{\frac{\left[5M_B^{*2} - E^*(\mathbf{p}')E^*(\mathbf{p}) + \mathbf{p}'\cdot\mathbf{p}\right]}{4M_B^{*2}} \cdot\left[M_B^{*2} - E^*(\mathbf{p}')E^*(\mathbf{p}) + \mathbf{p}'\cdot\mathbf{p}\right]\right\}\Delta_\eta(\mathbf{k}), \quad \text{(A4)}$$

and for the pion

$$\Xi_B^\pi = -\frac{2M_B^{*2}\left[\frac{g_A}{2f_\pi} F_\pi(\mathbf{k}^2)\right]^2}{E^*(\mathbf{p})E^*(\mathbf{p}')} \times \left\{M_B^{*2} - E^*(\mathbf{p})E^*(\mathbf{p}') + \mathbf{p}'\cdot\mathbf{p}\right\}\Delta_\pi(\mathbf{k}), \quad \text{(A5)}$$

where $E^*(\vec{p}) = \sqrt{\vec{p}^{\,2} + M_B^{*2}}$. In the above integrands we expand the terms in the braces multiplied by the propagator to isolate the momentum-independent pieces and multiply these contact terms by the variable ξ, which we use to investigate the consequences of contact subtraction. We emphasize here the importance of subtraction of the momentum-independent piece, which when transformed to configuration space corresponds to a δ function. In this manner our subtraction is implemented by the variable ξ, such that $\delta(\vec{r}) \mapsto \xi \times \delta(\vec{r})$. The removal of the contact terms is a common procedure owing to the fact that these contact terms represent very short-range, effectively zero-range, correlations between the baryons, which is not consistent in this model, which treats the baryons as clusters of quarks and not as pointlike objects. We give this explicitly for the vector-vector piece of the vector

mesons:

$$\frac{2M_B^{*2} - E^*(p')E^*(p) + \vec{p}' \cdot \vec{p}}{\vec{k}^2 + m_\eta^2} = \frac{2M_B^{*2} - p' \cdot p}{\vec{k}^2 + m_\eta^2} \simeq \frac{M_B^{*2} - \frac{\vec{k}^2}{2}}{\vec{k}^2 + m_\eta^2}$$
$$= \frac{M_B^{*2}}{\vec{k}^2 + m_\eta^2} - \frac{1}{2}\frac{\vec{k}^2}{\vec{k}^2 + m_\eta^2} = \frac{M_B^{*2} + m_\eta^2/2}{\vec{k}^2 + m_\eta^2} - \frac{1}{2}\xi. \quad \text{(A6)}$$

The remaining subtractions follow in the same manner.

[1] B. ter Haar and R. Malfliet, Phys. Rep. **149**, 207 (1987); E. N. E. van Dalen, C. Fuchs, and A. Faessler, Nucl. Phys. A **744**, 227 (2004); F. de Jong and H. Lenske, Phys. Rev. C **57**, 3099 (1998).

[2] J. Cugnon, P. Deneye, and A. Lejeune, Z. Phys. A **328**, 409 (1987); W. Zuo, A. Lejeune, U. Lombardo, and J. F. Mathiot, Eur. Phys. J. A **14**, 469 (2002); I. Bombaci and U. Lombardo, Phys. Rev. C **44**, 1892 (1991); B. D. Day and R. B. Wiringa, *ibid.* **32**, 1057 (1985); M. Baldo, G. F. Burgio, and H.-J. Schulze, *ibid.* **61**, 055801 (2000); I. Vidana, A. Polls, A. Ramos, L. Engvik, and M. Hjorth-Jensen, *ibid.* **62**, 035801 (2000).

[3] A. Akmal, V. R. Pandharipande, and D. G. Ravenhall, Phys. Rev. C **58**, 1804 (1998); A. Mukherjee and V. R. Pandharipande, *ibid.* **75**, 035802 (2007).

[4] A. Fabricioni and S. Fantoni, Phys. Lett. B **298**, 263 (1993); C. Bisconti, F. A. de Saavedra, G. Co', and A. Fabrocini, Phys. Rev. C **73**, 054304 (2006).

[5] Y. Dewulf, W. H. Dickhoff, D. Van Neck, E. R. Stoddard, and M. Waroquier, Phys. Rev. Lett. **90**, 152501 (2003).

[6] T. Frick and H. Müther, Phys. Rev. C **68**, 034310 (2003).

[7] B. S. Pudliner, V. R. Pandharipande, J. Carlson, S. C. Pieper, and R. B. Wiringa, Phys. Rev. C **56**, 1720 (1997); K. E. Schmidt and S. Fantoni, Phys. Lett. B **446**, 99 (1999); J. Carlson, J. Morales, Jr., V. R. Pandharipande, and D. G. Ravenhall, Phys. Rev. C **68**, 025802 (2003); S. Gandolfi, F. Pederiva, S. Fantoni, and K. E. Schmidt, Phys. Rev. Lett. **99**, 022507 (2007); S. Gandolfi, A. Yu. Illarionov, S. Fantoni, F. Pederiva, and K. E. Schmidt, *ibid.* **101**, 132501 (2008); S. Gandolfi, A. Yu. Illarionov, K. E. Schmidt, F. Pederiva, and S. Fantoni, Phys. Rev. C **79**, 054005 (2009).

[8] K. Hebeler and A. Schwenk, Phys. Rev. C **82**, 014314 (2010).

[9] K. Hebeler, J. M. Lattimer, C. J. Pethick, and A. Schwenk, Phys. Rev. Lett. **105**, 161102 (2010).

[10] M. Dutra, O. Lourenco, J. S. Sa Martins, A. Delfino, J. R. Stone, and P. D. Stevenson, Phys. Rev. C **85**, 035201 (2012).

[11] P. A. M. Guichon, Phys. Lett. B **200**, 235 (1988).

[12] P. A. M. Guichon, K. Saito, E. N. Rodionov, and A. W. Thomas, Nucl. Phys. A **601**, 349 (1996).

[13] K. Tsushima, K. Saito, and A. W. Thomas, Phys. Lett. B **411**, 9 (1997); **421**, 413 (1998).

[14] K. Tsushima, K. Saito, J. Haidenbauer, and A. W. Thomas, Nucl. Phys. A **630**, 691 (1998).

[15] P. A. M. Guichon, A. W. Thomas, and K. Tsushima, Nucl. Phys. A **814**, 66 (2008).

[16] K. Saito, K. Tsushima, and A. W. Thomas, Prog. Part. Nucl. Phys. **58**, 1 (2007).

[17] P. A. M. Guichon and A. W. Thomas, Phys. Rev. Lett. **93**, 132502 (2004).

[18] P. A. M. Guichon, H. H. Matevosyan, N. Sandulescu, and A. W. Thomas, Nucl. Phys. A **772**, 1 (2006).

[19] J. Rikovska Stone, P. A. M. Guichon, H. H. Matevosyan, and A. W. Thomas, Nucl. Phys. A **792**, 341 (2007).

[20] G. Krein, A. W. Thomas, and K. Tsushima, Nucl. Phys. A **650**, 313 (1999).

[21] T. Miyatsu, T. Katayama, and K. Saito, Phys. Lett. B **709**, 242 (2012).

[22] B. D. Serot and J. D. Walecka, Adv. Nucl. Phys. **16**, 1 (1986).

[23] A. Bouyssy, J. F. Mathiot, N. Van Giai, and S. Marcos, Phys. Rev. C **36**, 380 (1987).

[24] E. Massot, J. Margueron, and G. Chanfray, Europhys. Lett. **97**, 39002 (2012).

[25] J. J. de Swart, Rev. Mod. Phys. **35**, 916 (1963); **37**, 326(E) (1965).

[26] T. Miyatsu and K. Saito, Few Body Syst. **54**, 1591 (2013).

[27] W. Bentz and A. W. Thomas, Nucl. Phys. A **696**, 138 (2001).

[28] R. A. Williams and C. Puckett-Truman, Phys. Rev. C **53**, 1580 (1996).

[29] J. Beringer *et al.* (Particle Data Group Collaboration), Phys. Rev. D **86**, 010001 (2012).

[30] T. A. Rijken, M. M. Nagels, and Y. Yamamoto, Prog. Theor. Phys. Suppl. **185**, 14 (2010).

[31] J. P. Blaizot, Phys. Rep. **64**, 171 (1980).

[32] S. Shlomo, V. M. Kolomietz, and G. Colo, Eur. Phys. J. A **30**, 23 (2006).

[33] J. R. Stone, N. J. Stone, and S. A. Moszkowski, Phys. Rev. C **89**, 044316 (2014).

[34] M. Farine, J. M. Pearson, and F. Tondeur, Nucl. Phys. A **615**, 135 (1997).

[35] I. Tews, T. Kruger, K. Hebeler, and A. Schwenk, Phys. Rev. Lett. **110**, 032504 (2013).

[36] K. Hebeler and R. J. Furnstahl, Phys. Rev. C **87**, 031302(R) (2013).

[37] C. J. Horowitz and J. Piekarewicz, Phys. Rev. Lett. **86**, 5647 (2001).

[38] M. B. Tsang, J. R. Stone, F. Camera, P. Danielewicz, S. Gandolfi, K. Hebeler, C. J. Horowitz and J. Lee *et al.*, Phys. Rev. C **86**, 015803 (2012).

[39] I. Vidana, C. Providencia, A. Polls, and A. Rios, Phys. Rev. C **80**, 045806 (2009).

[40] S. Gandolfi, J. Carlson, and S. Reddy, Phys. Rev. C **85**, 032801 (2012).

[41] P. Danielewicz, R. Lacey, and W. G. Lynch, Science **298**, 1592 (2002).

[42] N. K. Glendenning, *Compact Stars: Nuclear Physics, Particle Physics, and General Relativity*, 2nd ed. (Springer, New York, 2000).

[43] J. R. Stone and P.-G. Reinhard, Prog. Part. Nucl. Phys. **58**, 587 (2007).

[44] M. Dutra, O. Lourenço, B. V. Carlson, A. Delfino, D. P. Menezes, S. S. Avancini, J. R. Stone, and C. Providncia, and S. Typel, AIP Conf. Proc. **1529**, 238 (2013).
[45] H. Sagawa, S. Yoshida, G.-M. Zeng, J.-Z. Gu, and X.-Z. Zhang, Phys. Rev. C **76**, 034327 (2007); **77**, 049902(E) (2008).
[46] L.-W. Chen, B.-J. Cai, C. M. Ko, B.-A. Li, C. Shen, and J. Xu, Phys. Rev. C **80**, 014322 (2009).
[47] J. Treiner, H. Krivine, O. Bohigas, and J. Martorell, Nucl. Phys. A **371**, 253 (1981).
[48] R. C. Nayak, J. M. Pearson, M. Farine, P. Gleissl, and M. Brack, Nucl. Phys. A **516**, 62 (1990).
[49] J. D. Carroll, AIP Conf. Proc. **1374**, 205 (2011).
[50] R. C. Tolman, Proc. Natl. Acad. Sci. U.S.A. **20**, 169 (1934); J. R. Oppenheimer and G. M. Volkov, Phys. Rev. **55**, 374 (1939).
[51] G. Baym, C. Pethick, and P. Sutherland, Astrophys. J. **170**, 299 (1971).
[52] P. Demorest *et al.*, Nature (London) **467**, 1081 (2010).
[53] J. Antoniadis, P. C. C. Freire, N. Wex, T. M. Tauris, R. S. Lynch, M. H. van Kerkwijk, M. Kramer, C. Bassa *et al.*, Science **340**, 6131 (2013).
[54] A. W. Steiner, J. M. Lattimer, and E. F. Brown, Astrophys. J. **722**, 33 (2010).
[55] S. Guillot, M. Servillat, N. A. Webb, and R. E. Rutledge, Astrophys. J **772**, 7 (2013).
[56] Ph. Podsiadlowski, J. D. M. Devi, P. Lasaffre, J. C. Miller, W. G. Newton, and J. R. Stone, Mon. Not. R. Astron. Soc. **361**, 1243 (2005).
[57] F. S. Kitaura, H.-Th. Janka and W. Hillebrant, Astron. Astrophys. **450**, 345 (2006).
[58] T. Katayama, T. Miyatsu, and K. Saito, Astrophys. J. Suppl. **203**, 22 (2012).
[59] T. Miyatsu and K. Saito, Prog. Theor. Phys. **122**, 1035 (2009).
[60] S. Weissenborn, D. Chatterjee, and J. Schaffner-Bielich, Phys. Rev. C **85**, 065802 (2012).
[61] S. Weissenborn, D. Chatterjee, and J. Schaffner-Bielich, Nucl. Phys. A **881**, 62 (2012).
[62] K. Masuda, T. Hatsuda, and T. Takatsuka, Prog. Theor. Exp. Phys. **2013**(7), 073D01 (2013).
[63] K. Masuda, T. Hatsuda, and T. Takatsuka, Astrophys. J. **764**, 12 (2013).
[64] D. Blaschke, D. E. Alvarez Castillo, S. Benic, G. Contrera, and R. Lastowiecki, PoS Confinement X, 249 (2012), arXiv:1302.6275 [hep-ph].
[65] J. Schaffner-Bielich, Nucl. Phys. A **835**, 279 (2010).
[66] F. Weber, Prog. Part. Nucl. Phys. **54**, 193 (2005).